Chemical Geology 584 (2021) 120551

Contents lists available at ScienceDirect

Chemical Geology

journal homepage: www.elsevier.com/locate/chemgeo

Uranium remobilisation in anoxic deep rock-groundwater system in response to late Quaternary climate changes – Results from Forsmark, Sweden

Juhani Suksi [a,*,1], Eva-Lena Tullborg [b], Ivan Pidchenko [c,d,e,2], Lindsay Krall [f], Björn Sandström [g], Kai Kaksonen [a,3], Tonya Vitova [e], Kristina O. Kvashnina [c,d], Jörg Göttlicher [h]

[a] Department of Chemistry, Radiochemistry Unit, University of Helsinki, Helsinki, Finland
[b] Terralogica AB, Östra Annekärrsvägen 17, SE-443 72 GRÅBO, Sweden
[c] Rossendorf Beamline at ESRF – The European Synchrotron, CS40220, 38043 Grenoble Cedex 9, France
[d] Helmholtz-Zentrum Dresden-Rossendorf, Institute of Resource Ecology, P.O. Box 510119, D-01314 Dresden, Germany
[e] Institute for Nuclear Waste Disposal (INE), Karlsruhe Institute of Technology, PO 3640, 76021 Karlsruhe, Germany
[f] SKB, Stockholm, Sweden
[g] WSP Sverige AB, Göteborg, Sweden
[h] Institute for Photon Science and Synchrotron Radiation (IPS), Karlsruhe Institute of Technology, P.O. 3640, D-76021 Karlsruhe, Germany

ARTICLE INFO

Editor: Dr Christian France-Lanord

Keywords:
U mobility
U redistribution
U series modelling
Redox conditions
Groundwater
Fracture coatings
Glaciation cycles
Climate changes

ABSTRACT

Unusually high uranium (U) concentrations (up to 175 μg/L) have been measured in groundwater at depths between 400 and 650 m at the Forsmark site, eastern Sweden. Since it is unlikely that such high concentrations formed under the stagnant and low redox groundwater conditions that currently prevail, this study employs U-series isotopes to understand how the recent evolution (<1 Ma) of the flow system has influenced the observed U distribution. Material from fractures as deep as 700 m along the assumed flow route was subject to U-series disequilibrium (USD) measurements, as well as sequential extractions (SE) and U redox-state analyses that revealed the U-series activity ratios in the bulk and soluble fraction of the fracture precipitates. Uranium isotope data collected over several years of annual groundwater monitoring were scrutinized to evaluate the U sources and U exchange in fractures located in high-U groundwater sections. Numerical simulations with the experimental data were used to study evolution of U-series isotope composition in a fracture in the highest U section at ~500 m depth under various U mobility scenarios. The results show that U redistribution in fractures with certain dissolution/deposition flux ratios during periodic water intrusions, driven by glaciation and deglaciation events during the last 120 ka, can explain the U anomaly in the groundwater.

1. Introduction

Natural U in deep groundwater has been extensively studied, for instance, in connection to the search for suitable locations for final disposal of spent nuclear fuel (SNF) (Gascoyne, 1997; Laaksoharju et al., 2009; Smellie et al., 2008; Posiva, 2011). Typically, U concentrations in these studies decrease from several hundred μg/L in dilute near-surface groundwater to around 1 μg/L in reducing deep groundwater environments (Gascoyne, 1997). However, during the SNF repository siting investigations at Forsmark (SKB, 2008) on the east coast of Sweden, 120 km north of Stockholm (Fig. A1 in Supplementary Material (SM)) the concentration-depth profile showed separate peaks, with the highest U concentration of 175 μg/L in one section at around 500 m depth. The finding was unexpected because the redox potential (E_h) is measurably negative (ca. -190 mV) and dissolved Fe(II) is present (Smellie et al., 2008).

It is unlikely that the U concentration profile was formed under the stagnant conditions that prevail in the Forsmark deep groundwater.

* Corresponding author.
E-mail address: suksi@elisanet.fi (J. Suksi).
[1] Current affiliation: DecServis Consulting Co., Yliskyläntie 7H 84, 00840 Helsinki, Finland.
[2] Current affiliation: Department of Biology and Environmental Science, Linnæus University, SE-39182 Kalmar, 39182, Sweden.
[3] Current affiliation: T-MEDIA, Eteläinen Makasiinikatu 4 A, FIN-00130, Finland.

https://doi.org/10.1016/j.chemgeo.2021.120551
Received 30 August 2020; Received in revised form 8 September 2021; Accepted 23 September 2021
Available online 27 September 2021

Nevertheless, the anomaly has been linked to U remobilisation triggered by intrusion of chemically different waters (Smellie et al., 2008; Sandström et al., 2008; Krall et al., 2020). Mineralogical investigations at the site revealed several generations of U minerals, which formed sporadic U(VI) sources throughout the bedrock following geologically early episodes of hydrothermal fluid circulation (Krall et al., 2015; Krall et al., 2019). It was also shown that U remobilisation in fractures could have occurred recently, for instance during the Quaternary including the Holocene. Similar observations of recent U mobility have been reported elsewhere in the Fennoscandian Shield (Löfvendahl and Holm, 1981; Blomqvist et al., 2000; Rasilainen et al., 2003; Read et al., 2008).

The persistence of unusually high U concentrations in anoxic groundwater conditions at 500 m depth several thousand years after the last water intrusion (the Littorina Sea in Fennoscandia) is explained by formation of the $Ca_2UO_2(CO_3)_3^0$ complex (Krall et al., 2020), which has been identified in the groundwater (cf. Tullborg et al., 2017). The existence and stability of the $Ca_2UO_2(CO_3)_3^0$ complex in oxic U mining waste waters has been earlier reported by Bernhard et al. (2001). Laboratory experiments have demonstrated persistence of U(VI) tricarbonate complexes in mildly reducing conditions owing to their high thermodynamic stability (Geckeis et al., 2013 and references therein). Importantly, the finding in Forsmark is the first one made in an anoxic

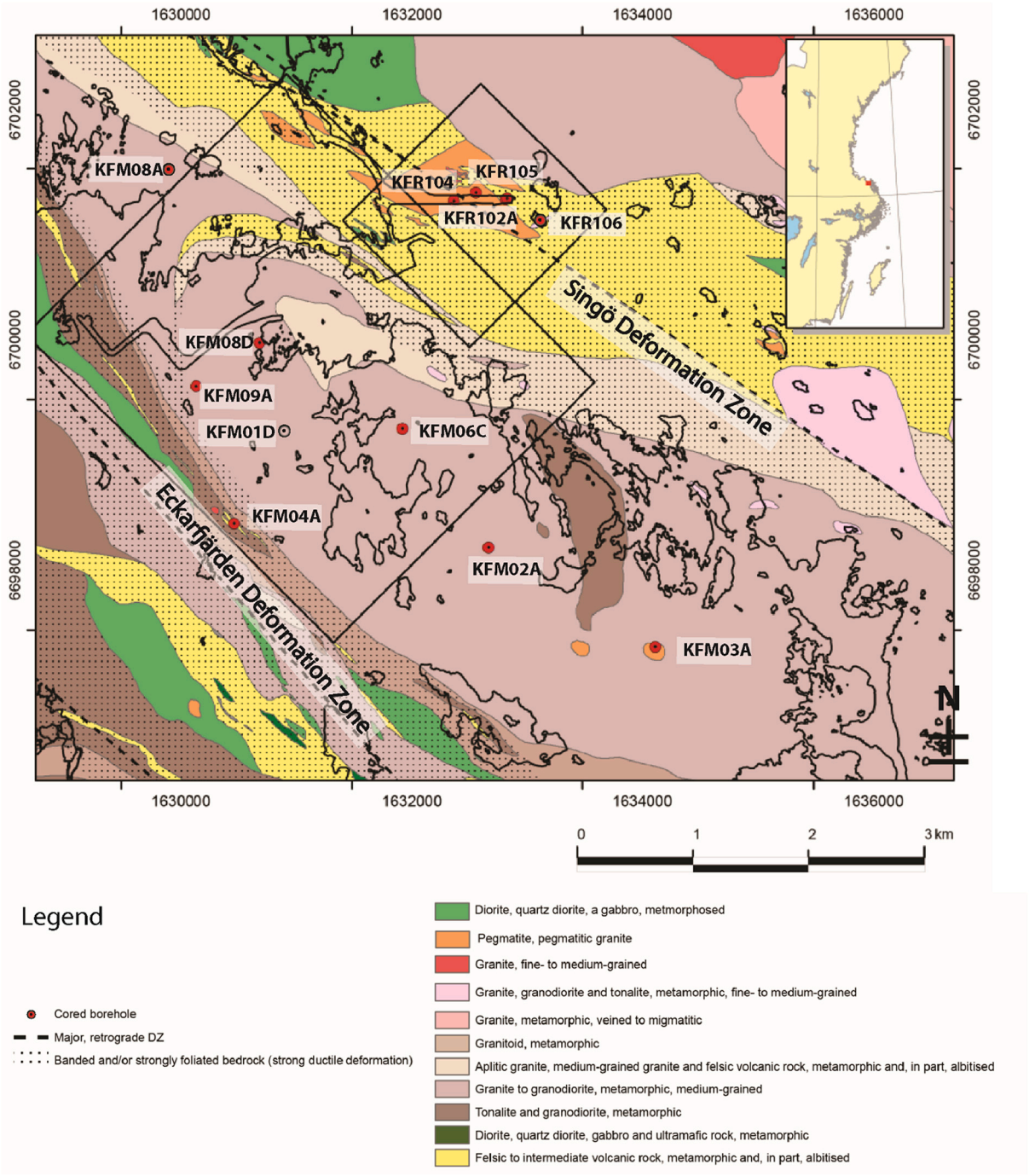

Fig. 1. Bedrock geological map of Forsmark (Stephens et al., 2008) with the map of Sweden inserted in top right corner (from Krall et al., 2019). Boreholes in which uranium mineral chemistry has been reported by Krall et al. (2015) and Sandström et al. (2011 and 2014) are shown. Current isotopic data are reported from boreholes KFR01, KFR102B, KFR104, KFR105, KFR106 (small square) and from KFM02A, KFM02B, KFM03A, KFM06C and KFM08D (large square).

deep groundwater environment.

The objective of the present study was to clarify the role of recent U redistribution in creating high U concentrations in the deep groundwater. To assess the U mobility along the assumed flow routes, fracture coatings from the upper part of the bedrock down to depths exceeding 700 m have been studied together with groundwater samples from relevant sections. Results of the U-series disequilibrium (USD) measurements and sequential extractions (SE) were used to characterize mobility of U. The redox state of U was further studied through anoxic extraction of selected fracture coatings. The results of one coating material were compared to synchrotron X-ray absorption spectroscopic (XAS) measurements. The unique U isotope data gained over several years' annual groundwater monitoring were used to test an approach to link the U source to the U isotope distribution in the groundwater. The modelling tool presented in Azzam et al. (2009) has been used to simulate U exchange and activity ratios in the fracture located in the highest U groundwater section. The model was constrained by the USD signatures measured in the fracture coating.

2. Site description

2.1. Geology

The Forsmark site, including the existing low- and intermediate-level waste repository (SFR) below the Baltic Sea, is characterized by Paleoproterozoic crystalline bedrock that has been affected by strong ductile deformation under amphibolite-facies metamorphic conditions (Fig. 1). The crystallization and deformation of the igneous rocks occurred between 1.9 and 1.8 Ga (Stephens, 2010 and references therein). The inner part of the Forsmark site is situated within a tectonic lens, which is surrounded by steeply dipping major fracture zones trending NNW-SSE (Stephens et al., 2008). Gently SE-dipping zones transect the volume between these steep zones.

Sandström et al. (2008, 2009) constrained the brittle deformational history of the site and presented four generations of fracture minerals, transitioning from Proterozoic and hydrothermal conditions to low temperature and possibly recent. Krall et al. (2015, 2019) studied the U—Pb geochronology and oxidation of uranium in response to these mineralisation events. The two main Proterozoic hydrothermal episodes, at ~1.6 Ga (Krall et al., 2019) and at 1.1–0.9 Ga (Sandström et al., 2009), are manifested by hematite-staining of the bedrock through oxidation of Fe(II). U oxidation and mobilisation are also preserved, with the initial precipitation of Ca-U(VI)-silicates at ~1.25 Ga (Krall et al., 2019).

During the Palaeozoic, fluids migrated downward from an organic-rich sedimentary overburden, which covered the Palaeoproterozoic crystalline rocks of the area at the time (Cederbom et al., 2000). Sulphide minerals including pyrite and galena, in addition to quartz, calcite, corrensite, analcime, and adularia were formed, and U(IV) precipitated in the upper part of the bedrock (Krall et al., 2015). Despite the overall reducing conditions, Krall et al., (2019) documented uranophane and haiweeite of Palaeozoic ages (400–300 Ma), which is consistent with ^{40}Ar—^{39}Ar dates 456–277 Ma for closely associated adularia (Sandström et al., 2009). Rb—Sr datings of fracture albite also support Devonian-Carboniferous ages, but even younger calcite has been dated to the Jurassic (LA-ICP-MS U—Pb dating; Drake et al., 2017).

The youngest fracture mineralisation consists of calcite, clay minerals and Fe-oxy-hydroxide that precipitated, at low temperature, in near surface fractures (Sandström et al., 2008, 2009). Due to the complexity of the samples, this mineralisation could not be dated but is possibly Quaternary in age and may relate to a U-mineral reactivation event(s).

2.2. Hydrogeology

Several cycles of glacial loading and unloading occurred during the Quaternary (cf. Näslund, 2010 and refences therein). These have influenced the hydraulic conductivity of the fractures with a proposed increase in hydraulic pressure during periods with advance or retreat of the ice and with large volumes of meltwater transported via fractures in the ice and tunnels below (Follin et al., 2008). The impact of deglaciation on the Baltic Sea boundaries is shown in SM Fig. A2.

The possibility that repeated marine transgressions and regressions influenced the area are considered likely, given the location close to the Baltic Sea coast and the flat topography. This, together with alternating periods of glaciation/deglaciation and permafrost, has caused extensive changes in the groundwater chemistry to depths greater than 500 m.

2.3. Hydrochemistry

More than fifty packed-off borehole sections at depth from 50 m down to 1000 m have been sampled for groundwater chemistry (Laaksoharju et al., 2008; Nilsson et al., 2011), and many sections have subsequently been annually monitored to evaluate the stability in the groundwater chemistry over time.

The hydrochemical model outlined for the area (Laaksoharju et al., 2008; Smellie et al., 2008; Nilsson et al., 2011) describes several groundwater types with different origin and residence times. The oldest is a brackish-to-saline water (>6000 mg/L Cl) that generally shows low concentrations of Mg, K, SO_4 and HCO_3 and is therefore categorised as a non-marine-type groundwater. This is an old saline water that has resided in the bedrock for up to several hundred thousand years and has partly mixed with a water with low $\delta^{18}O$ that originated from glacial meltwater of the last or earlier glaciations (Smellie et al., 2008). The high hydraulic head created when meltwater enters the bedrock can inject the glacial meltwater to great depth. At Forsmark, glacial remnants were indicated down to at least 1000 m depth. It is assumed that the upper several hundreds of meters of the bedrock fractures were almost replaced with this diluted water. When the area was subsequently deglaciated, the hydraulic head was diminished (Follin et al., 2008). This, together with the changes in stress pattern due to isostatic rebound of the crust, led to the formation of isolated pockets with meltwater in certain bedrock fractures (Nilsson et al., 2011).

During the Holocene, the area was influenced by the evolution of the Baltic Sea (cf. Follin et al., 2008 and references therein; cf. SM Fig. A2) and especially by the increased inflow of Atlantic Sea water via the Öresund strait (between Sweden and Denmark). This stage is named the Littorina Sea, which at its peak some 7 to 6.5 ka ago had a salinity of 6000 mg/L (twice as high as today's salinity of the Baltic Sea off-shore Forsmark). The Littorina Sea transgression resulted in brackish sea water intrusion via the most conductive zones that intersected the seabed. Ancient sea water, mixed with glacial meltwater in the bedrock fractures, is detected as deep as 630 m. The resulting groundwater type is named “brackish marine-glacial”. Recent groundwater recharge of meteoric-type water is detected in the upper 50 to 100 m of the bedrock aquifer inland Forsmark, whereas present Baltic Sea water can be found in the upper 100 m of the sub-sea bedrock at SFR. The groundwater becomes anoxic in the upper 10 to 20 m (Smellie et al., 2008). Fig. 2 shows depth variation of key groundwater components, including Cl (salinity), Mg (indicator of sea water), $\delta^{18}O$ (low values indicate glacial meltwater), and Fe(II) (indicator of reducing/anoxic conditions).

3. Methods

3.1. Drill core sampling

3.1.1. Selection of samples

A general problem in water-rock interaction studies is to relate a specific fracture coating sample to the corresponding groundwater (cf. Tullborg et al., 2008). This often fails because the groundwater signature is inherited from a large fracture surface (a radius of tens of meters or more) or even several different fractures. The fracture mineral

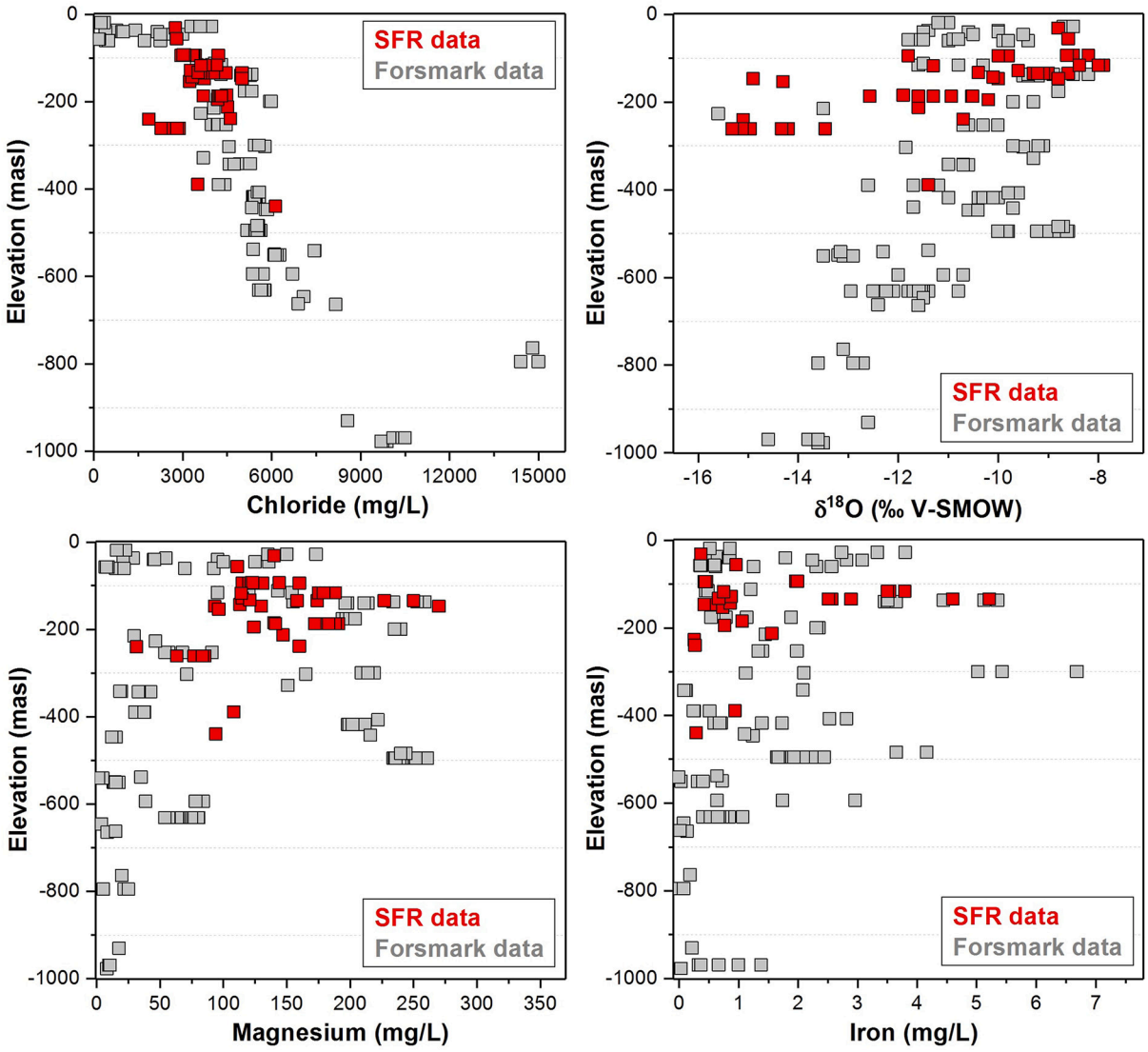

Fig. 2. Cl, $\delta^{18}O$, Mg and Fe (practically Fe^{2+}) in groundwater samples from Forsmark and the nearby SFR area plotted versus vertical depth given as elevation (m.a.s.l.). Data from SKB's database Sicada with monitoring data (SM part A: Groundwater chemistry data).

sample, in contrast, represents a few cm^2 and the flow-wetted surface assumed to have interacted with the groundwater may be even smaller. The fracture coating usually contains minerals precipitated during different time periods and different hydrochemical conditions. For the present study additional issues include the risk that U redox state was affected by handling and storage of the drill core. Also, large variation of U in fracture coatings, from less than one ppm up to several weight percent needs to be considered.

Based on challenges in the sampling the following different approaches were applied for sample selection (cf. Table 1).

1) To get fracture samples corresponding to groundwater samples information from flow logs and optical tele logging (BIPs stored in SKB's database, Sicada) were used. The samples include fracture coatings from e.g., drill cores KFM02A:423 m, KFM02A:513 m, and KFM03A:643 m where the high U groundwater has been sampled. These two boreholes penetrate a system of gently dipping, highly transmissive fracture zones. Unfortunately, flushing and grinding during the drilling has made it difficult to obtain undisturbed drill core samples from the most transmissive parts of the zones.
2) For the acquisition of redox-sensitive samples it was important to avoid artificial disturbances. Thus, in connection to the drilling of borehole KFR106, samples were vacuum-sealed and stored in a nitrogen glove box under an oxygen-free atmosphere (Sandström et al., 2011). Therefore, the sampling was performed before the core mapping, the flow logging, and the selection of sections for groundwater sampling.
3) To obtain samples with enough U to test different analytical techniques, additional samples were taken based on gamma logs (stored in SKB's database, Sicada) and handheld scintillometer.

To maximize the sample quality, triple tube drillings is strongly preferred. These drill cores are better preserved, and the loss of material due to flushing and grinding is usually limited. The KFM boreholes (inland Forsmark) were drilled (triple tube) between 2002 and 2007, whereas the KFR boreholes (below Baltic Sea) have two different series; the one starting with KFR01 drilled 1986–1987 (not triple tube) and the series from KFR101 to KFR106 drilled (with triple tube) 2008 to 2009. All samples included in the present study are listed alongside core length, elevation, and analytical methods applied in Table 1. Drill core samples from groundwater sections with repeated high U measurements are indicated in bold (Table 1).

Table 1
Sample information. U concentrations have been determined by ICP-MS. KFM refers to Forsmark and KFR to the low- and intermediate-level waste repository SFR. Bulk U-series analyses were done for all samples. Samples for other analyses and analytical tools are indicated. Drill core samples from groundwater sections with repeated high U measurements are indicated (bold).

Drill core	Core length, m	Elevation, m.a.s.l.	Transmissivity, m^2/s [1]	U ppm	SE[2]	Ox[3]	Comment
Vacuum sealed samples from KFR106 stored and handled in N2-glove box							
KFR106	16.62–16.97	-14.57	10^{-7} to 10^{-5}	44–58	x	x	X2[4]
KFR106	68.41–68.46	-63.18	10^{-7} to 10^{-5}	4.53			
KFR106	85.13–85.52	-78.87	10^{-7} to 10^{-5}	232			U-phosp[5]
KFR106	86.88–87.33	-80.51	$<10^{-11}$	142	x	x*	U-phosp[5]
KFR106	100.56–101.08	-93.33	10^{-7} to 10^{-5}	6.95			
KFR106	112.91–113.35	−104.90	10^{-7} to 10^{-5}	5.96			
KFR106	131.42–131.71	−122.22	$<10^{-11}$	16.6			
KFR106	154.22–154.99	−143.54	10^{-7} to 10^{-5}	3.03			
KFR106	156.11–156.20	−145.31	10^{-7} to 10^{-5}	15.4			
KFR106	188.14–188.56	−175.24	10^{-7} to 10^{-5}	24–137			X3[4]
KFR106	229.59–230.11	−213.96	$<10^{-11}$	10.2			
KFR106	244.83–245.35	−228.19	$<10^{-11}$	3.0			
KFR106	262.48–262.97	−244.67	10^{-7} to 10^{-5}	2.03	x	x	
KFR106	299.77–300.00	−279.48	$<10^{-11}$	7.6–21.1	x	x	X2[4], Pitchb[5]
Samples from sections with increased gamma levels detected by geophysical logging							
KFR01	26.35–26.52	-70.80	10^{-11} to 10^{-8}	110			
KFR102B	104.37–104.51	-82.07	10^{-11} to 10^{-8}	3610			
KFR104	21.57–21.66	-14.64	10^{-11} to 10^{-8}	19,223			U-Ca oxide[5]
KFR104	21.34–21.47	-14.83	10^{-11} to 10^{-8}	1311	x		U-Ca-Oxide[5]
KFR104	43.53–43.76	-32.75	10^{-11} to 10^{-8}	117			
KFR104	107.83	-84.81	10^{-11} to 10^{-8}	174			
KFR105	16.58–16.84	−109.72	$<10^{-11}$	349			
KFR105	51.73–51.87	−115.75	$<10^{-11}$	3			
KFM04A	899.68–899.82	−724.60	$<10^{-11}$	20.3			
Samples from sections with U analysed in groundwater							
KFR105	45.54–45.87	−114.70	10^{-11} to 10^{-8}	5.84			6–27 ppb[6]
KFM02A	**513.21–513.42**	**−504.13**	**10^{-7} to 10^{-5}**	**31.5**			**63–172 ppb[6]**
KFM02A	**423.48–423.64**	**−414.79**	**10^{-11} to 10^{-8}**	**10.5**			**24–46 ppb[6]**
KFM02B	420.03–420.25	−406.59	10^{-7} to 10^{-5}	3259			4–5 ppb[6]
KFM03A	**643.95–644.05**	**−633.32**	**10^{-7} to 10^{-5}**	**1587**	**x**		**16–52 ppb[6]**
KFM06C	537.27–537.50	−436.21	10^{-11} to 10^{-8}	4.37			44 ppb[6]
KFM06C	537.72–537.86	−436.56	10^{-11} to 10^{-8}	1674			44 ppb[6]
KFM08D	676.23–676.35	−542.96	10^{-11} to 10^{-8}	19.9			0.2–1.5[6]
KFM08D	832.35–832.55	−664.36	10^{-11} to 10^{-8}	15.03			0.5–1.5 [6]

For location of the boreholes see Fig. 1.
1 = Transmissivities from PFL logging (SKB database Sicada).
2 = Sequential extraction analyses (SE) performed.
3 = Oxidation state analyses performed: anoxic extraction and L_3 edge HERFD-XANES spectroscopy (x*).
4 = Number of subsamples analysed from the same fracture coating.
5 = U-phase detected in SEM see Sandström et al., 2011 and 2014. Detailed studies by Krall et al., 2015 identified an Y and P rich coffinite in near-surface fractures, which may relate to the U-phosphate.
6 = U-concentration in groundwater from corresponding borehole section, data from SKB's database Sicada.

3.1.2. Sample description

Generally, the fracture coatings consist of a mixture of chlorite, calcite, adularia, and clay minerals of corrensite and/or smecitite-illite, deposited at different times and variably affected by secondary processes. Small amounts of hematite, laumontite, pyrite, barite, asphaltite and in some fractures Fe-oxyhydroxide, are also present. However, there is a large variation in coverage and mixtures of fracture minerals on the fracture surfaces. Typical coating thicknesses range from 0.5 to a few mm. Mineralogical analyses have been performed for all samples from KFR106 (Sandström et al., 2011) and KFR104 (Sandström et al., 2014). Uranium in the fracture coatings is incorporated into and associated with the above-mentioned minerals. In a few cases, precipitation of pure U phases is found as grains or thin precipitates (cf. Krall et al., 2015, 2019). In the dataset presented here, specific U-minerals were difficult to identify, with a few exceptions (Table 1). Details of some samples are shown in SM Figs. A3 and A4.

The fracture coatings were gently scratched off the core surfaces using a steel knife, and 50 to 300 mg was obtained per sample. The small sample volumes and the complex history of the fracture coatings (cf. Section 2.1) yields heterogeneity which is difficult to avoid. Since homogenisation by crushing would have created new mineral surfaces that would adversely affect the sequential extraction results, particle size vary between samples.

3.2. Experimental and analysis

3.2.1. Sequential extraction (SE)

SE is often used to study dispersion and bioavailability of harmful metals in the environment, as documented and discussed in the literature (cf. Rauret and Quevauviller, 1992). In this study, the method was used to evaluate mobile fraction of U in fracture coating material. Eight fracture coating samples each yielded enough material for SE analyses. In the procedure, sample material was successively extracted, starting with water, to determine weakly and more tightly bound U.

The water used was tap water (TW) which is a lake water that has been treated for drinking water and here represents oxygenated dilute surface water. Main cations Na (6 mg/L), Ca (27 mg/L), Mg (~ 2 mg/L) and anions HCO_3 (30–60 mg/L), Cl (6 mg/L), SO_4 (65–348 mg/L). TW extractions were performed by shaking 120–250 mg of sample material in 10 ml in air at room temperature for two hours. The pH of the TW extractions was 7.5. Solid part was separated using 0.45 μm filter.

Immediately after the water extraction, sample material was exposed to ammonium acetate buffer solution (pH = 4.8, 1 M NH_4Ac + 0.02 M EDTA) to dissolve the soluble U(VI) phases (cf. Bolle et al., 1988). EDTA

was used to keep dissolved Th in solution. In the last two steps, extractions in 6 M HCl and *Aqua Regia* were performed to remove U-series nuclides from the more resistant phases. The mineral residue is usually U-poor but may contain excess ^{234}U and ^{230}Th recoiled from U-rich phases. This excess is proportional to the timing of U deposition (Suksi and Rasilainen, 1996).

An additional water leaching experiment was performed with synthetic groundwater (SGW), which was prepared to correspond the brackish marine-glacial groundwater type usually found at 500 m in the most transmissive zones were also the highest U has been measured. Main cations were Na (2000 mg/L), Ca (900 mg/L), and anions HCO_3 (125 mg/L), Cl (5500 mg/L), SO_4 (200 mg/L), and pH adjusted to 7.5. In the extraction, sample material of about 100 mg was stirred for 20 min in 10 ml of deoxygenated water in a glove box ($O_2 < 2$ ppm) at 25 °C.

3.2.2. Oxidation state of solid U

Uranium oxidation states were separated using ion-chromatography. The principle of the method for separation is based on the distinct distribution coefficients that U(IV) and U(VI) complexes formed in 4.5 M HCl have for a Dowex1 × 4 anion-exchange resin. Whereas negatively charged U(VI) complexes are retained by the anion exchange resin, positively-charged U(IV)-chloride complexes pass through the column.

The material was treated for 10 min in 20 ml of 4.5 M HCl + 0.03 M HF solution (bubbling with Ar), where U(IV)- and U(VI)-chloro complexes were formed and maintained until analysed. The leachate was immediately filtered over a 0.2 μm Millipore membrane, then loaded in an anion exchange column (Dowex 1 × 4, 50–100 mesh). The U(IV) fraction was collected in the first 20 ml fraction and U(VI), retained in the column, was eluted with 20 ml of 0.1 M HCl (Pidchenko et al., 2013 and references therein). The leached fracture material was subsequently treated with strong HNO_3, to dissolve the residual U, considered to be insoluble U(IV). All leachates were determined by alpha-spectrometry. The uncertainties of the procedure include the possibility of U redox perturbations during material leaching in acid, for instance by Fe(II) and/or Fe(III) species released during the leaching. To correct for the oxidation or reduction of U, a U redox tracer, such as ^{236}U, was added.

3.2.3. ^{238}U-series disequilibrium (USD) measurements

For the alpha-spectrometry analyses, sample material (120–250 mg) was spiked with ^{236}U and ^{229}Th isotopic yield tracers and extracted in 20 ml hot *Aqua Regia* for 30 min. The leachate was filtered through a 0.2 μm Millipore membrane, prepared in 9 M HCl and loaded in Dowex 1 × 4 resin for U/Th separation. Finally, purified U and Th fractions were precipitated in CeF_3, which was mounted on a measurement plate for α-spectrometry. SE leachates were treated in hot concentrated HNO_3 to decompose organics before the α-spectrometry.

PIPS-detectors of 450 mm^2 area with a nominal resolution of 20 keV were used. Counting statistic (1σ) varied 2.0–7.5%, 4.0–8.5% and 3.4–8.1% for the ^{234}U/^{238}U, ^{230}Th/^{238}U and ^{230}Th/^{234}U activity ratios, respectively. Reproducibility of the method was tested repeatedly by analysing 50 mg of a certified U/Th-mineral reference DL-1a where the ^{238}U-decay series is known to be in secular equilibrium (Steger and Bowman, 1980). Equilibrium value for ^{234}U/^{238}U and ^{230}Th/^{234}U ARs ~1 was obtained with the accuracy of 2%.

The synthetic groundwater extraction leachates were digested in hot *Aqua Regia* for isotopic measurements by multi-collector inductively coupled plasma mass-spectrometry (MC-ICP-MS). An in-house ^{229}Th-^{233}U-^{236}U spike, prepared and calibrated by the Geological Survey of Finland, was added to the filtered solution (0.22 μm Millipore). U was separated from the solution using a TRU resin by Eichrom. Final leachates were evaporated nearly to dryness and prepared in 2% HNO_3. Solutions were diluted to U concentration between 20 and 30 ppb into a disposable 2 ml beaker in 1.0 to 1.5 ml 2% HNO_3. Measurements were carried out using a desolvator nebuliser, a 80 μl Meinhard concentric quartz nebuliser, and a Multi-Collector Inductively Coupled Plasma Mass Spectrometer (Nu Instruments™). Measurements were performed at the Geological Survey of Finland following a procedure described by Luo et al. (1997). U blank was in the 6 pg range. For details see SM part B.

3.3. Synchrotron-based techniques

Synchrotron methods to determine U oxidation state and mineralogy was performed for KFR106:86 m. This sample, taken from the upper part of the bedrock where the most intense leaching of U has occurred, was the only one to offer enough U-rich fracture coating material to enable a comparison between wet chemistry and mineralogical methods for determination of U oxidation states in the fracture material.

3.3.1. U L_3 edge high-energy resolution fluorescence-detected X-ray absorption near edge structure (HERFD-XANES) spectroscopy

U L_3 edge HERFD-XANES spectroscopy can clearly distinguish minor contributions of different U redox states in complex, environmentally relevant systems (Pidchenko et al., 2017; Rothe et al., 2019). For the measurements sample material and reference compounds were pressed into pellets with cellulose and packed into a gas-tight, dual-containment sample holder (10 and 13 μm polypropylene) in an Ar-glovebox and transported in a gas-tight container. The measurements were performed with a Johann type X-ray emission spectrometer at the ID26 beamline, ESRF, Grenoble, France (Glatzel and Bergmann, 2005). The ATHENA program from the IFFEFIT software package was used for the spectra evaluation (Ravel and Newville, 2005). For more details see SM part B.

3.3.2. Microfocus powder X-ray diffraction (μ-PXRD)

The μ-PXRD measurements were performed at the SUL-X beamline of KIT synchrotron radiation source in Karlsruhe, Germany (Goettlicher et al., 2013). Measurements were performed under air and room temperature. Data was analysed using the FIT2D program for radial integration of the Debye rings and DIFFRAC.EVA V3.1 (Bruker) program for background subtraction and diffraction peaks evaluation (Hammersley et al., 1996). For more details see SM part B.

3.4. Numerical simulation

The simulation was used to mimic natural U redistribution (U exchange between solid and solution) to evaluate the relation between U redistribution on fracture surface and elevated U concentrations in the groundwater. The model for U redistribution processes was reconstructed using information of the last glaciation-deglaciation episode. The redistribution was constrained using data from past groundwater conditions and site-specific experimental data. Radioactive decay and ingrowth equations, including a term for U input and output fluxes, was used to calculate the evolution of the U-series isotope composition as a function of time (cf. SM Part C). The description of the modelling tool can be found in Azzam et al., (2009). The approach is analogous to other U transport models reviewed in Chabaux et al. (2008).

4. Results

4.1. Groundwater U data

The groundwater evolution outlined in Section 2.3 has likely been a driving force for the current U distribution in the Forsmark groundwater. Generally, wide variation is observed in the U concentration (<1 μg/L to >175 μg/L) and the ^{234}U/^{238}U AR (1.5–6.5) (Fig. 3). The U concentration profile does not show decrease with depth; rather, the highest concentrations were measured in parts of the deep groundwater environment, a pattern that has persisted in annual time-series samples through the present including unpublished values from recent years, all presented in Fig. 3. High concentrations are generally associated with the brackish marine-glacial groundwater-type with negative E_h values (−140 to −190 mV) (Laaksoharju et al., 2008; Nilsson et al., 2011).

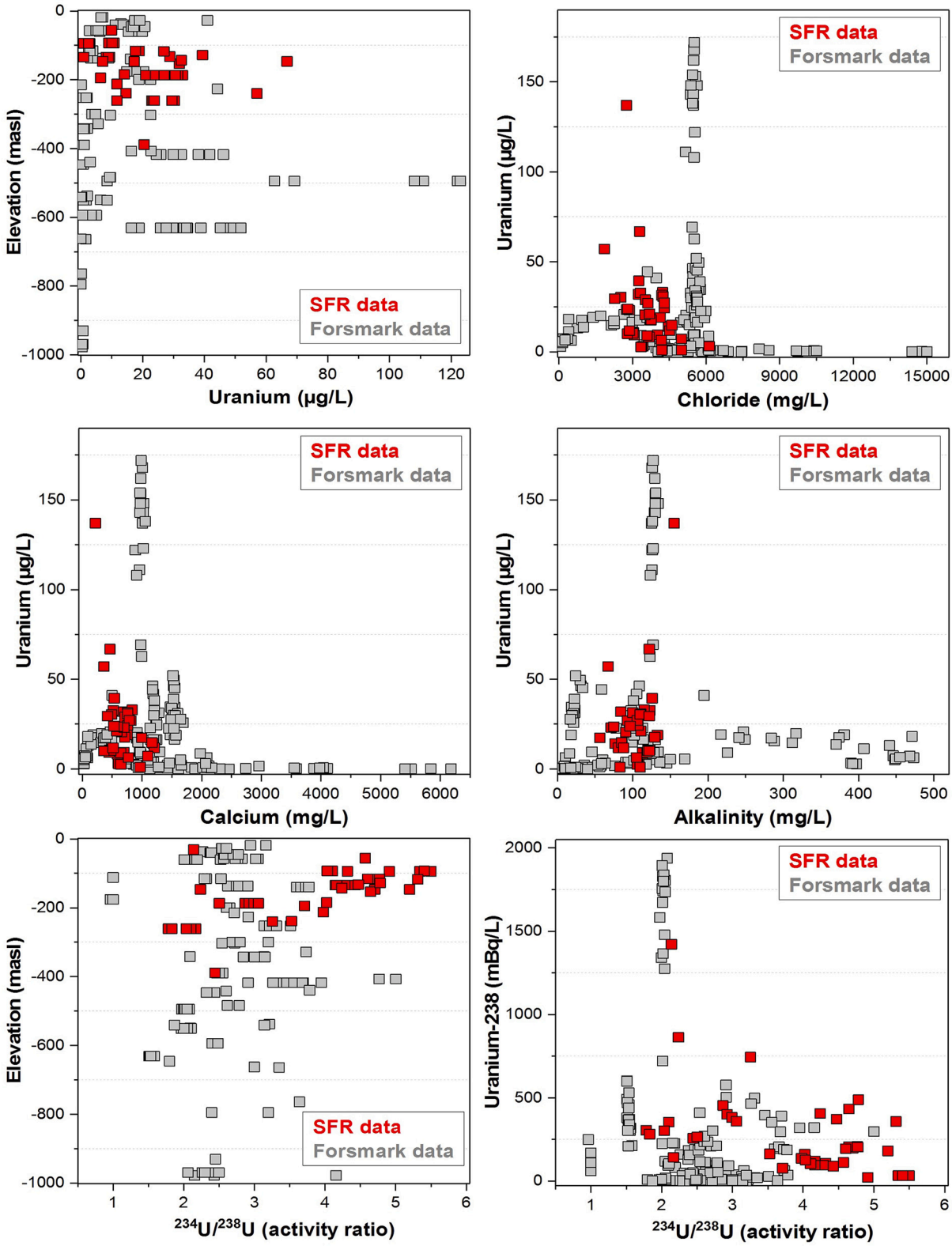

Fig. 3. U distribution as function of elevation (m.a.s.l.), Cl, Ca and alkalinity (practically HCO_3) in sampled groundwater sections. Two lower panels; $^{234}U/^{238}U$ (AR) versus elevation and ^{238}U. Data from SKB's database Sicada (SM part A: Groundwater data).

Since the ongoing recharge of meteoric or present Baltic Sea water influence only the upper 100 m the observed U concentration peaks below this depth relate to earlier recharge processes, such as that of glacial meltwater and the Littorina Seawater. In the highest U groundwater section (KFM02A:490–518 m), U oxidation state analyses showed a total dominance of U(VI) (Suksi and Salminen, 2007).

Annual groundwater monitoring of U isotopes, partly reported in Tullborg et al. (2017) has continued to produce new data. Three deep sections have been studied (KFM02A:411–442 m, KFM02A:490–518 m, and KFM03A:633–650 m). Time-series isotope activities (Bq/L) were

plotted ^{238}U versus ^{234}U (Fig. 4), and correlation trend lines were examined to evaluate U isotope release ratios (similar approach as Suksi et al., 2006). Good correlation was obtained in all three groundwater sections ($R^2 > 0.91$).

Trend lines from KFM02A:490–518 m and KFM03A:633–650 m groundwater sections showed perfect fit ($R^2 \sim 1$) despite the wide variation in concentrations between sampling occasions. Both trendlines intercepted the origin which reflects congruent dissolution of U, during which the isotopes do not fractionate. The trendline slope, or the $^{234}U/^{238}U$ release ratio, is the same as the $^{234}U/^{238}U$ AR for both, respective groundwater sections, (~2 and 1.5; SM Table A1), which suggests that U is supplied by one main source specific for each groundwater section.

Interestingly, the KFM02A:411–442 m trendline showed a weaker correlation and intercepted clearly above the origin (Fig. 4). The slope was different from the $^{234}U/^{238}U$ AR in this groundwater (~2 and 3.5, respectively), and the $^{234}U/^{238}U$ AR showed larger variations between sampling occasions (2.91–3.95). It is possible that inconsistent pumping and flow rates caused mixing of groundwaters with different U characteristics during the eight sampling occasions between 2005 and 2010.

4.2. U and USD in fracture coating material

4.2.1. Sequential extraction (SE) results

Total extractable U, studied in eight of the samples, varied from a few ppm to over 4000 ppm, indicating presence of U-rich phases in some of the fracture coatings. Large portions of the U occurred in an easily extractable form (water + NH_4Ac up to 80%) of which the water-soluble portion varied between 0.11 and 25% (Fig. 5 and SM Table B1).

The four samples from drill core KFR 106 were subject to leaching tests with two different waters (cf. Section 3.2.1). Interestingly, a larger portion of U was dissolved in the anoxic SGW (1.8–18%) compared with the oxic TW (0.1–10%) (Table 2). The higher solubility of U in the anoxic SGW was unexpected but can be due to its higher cation and complexing ion concentrations, which were similar to the high U groundwater section KFM02A:490–518 m. Bulk samples (whole fracture coating material) were analysed twice in a two-year interval on similar fracture material, first time followed by alpha-spectrometric and second time by MC-ICP-MS measurements (cf. Table 2). These two different sets of analyses were done to 1) check the reproducibility of results after considerable storage time and 2) obtain data with minimized errors for more precise analysis (cf. Table 2). In three of the fracture coatings the AqRg extractions showed good agreement in both U concentration and ARs, considering the uncertainty in alpha-spectrometry. For sample KFR106:262 m the differences were larger which can be due to the sample heterogeneity but partly also to the low U content in this sample (2.0 to 3.4 ppm).

While $^{234}U/^{238}U$ AR results from TW and SGW experiments show in general good agreement within 2–3 standard deviations (σ), noticeable variation was found in sample KFR106:262 m (Table 2). Both waters extracted U with the $^{234}U/^{238}U$ AR clearly over unity. For the near-surface sample (KFR106:17 m), the SGW leachate gave AR = 1.12, similar to that measured in the Baltic Sea water (Skwarzec et al., 2004). Water leachates from drill cores KFR106:86 m gave ARs 1.9–2.1, which

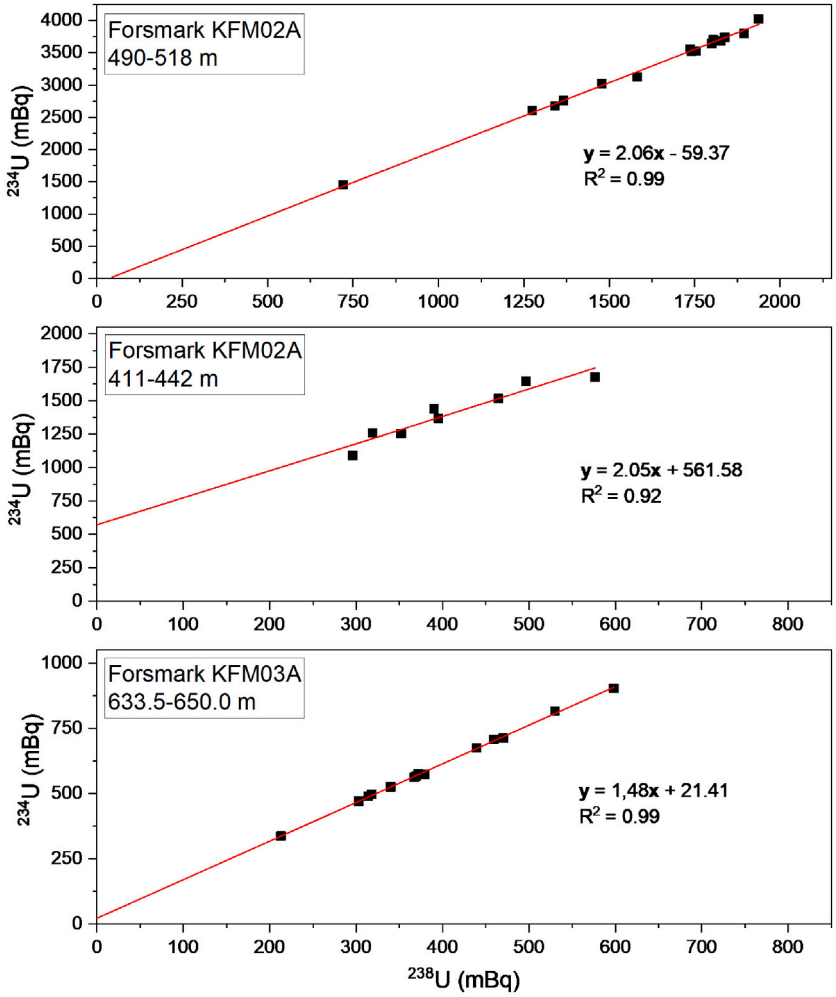

Fig. 4. ^{234}U—^{238}U correlation in the deep groundwater sections where elevated U concentrations have been measured.

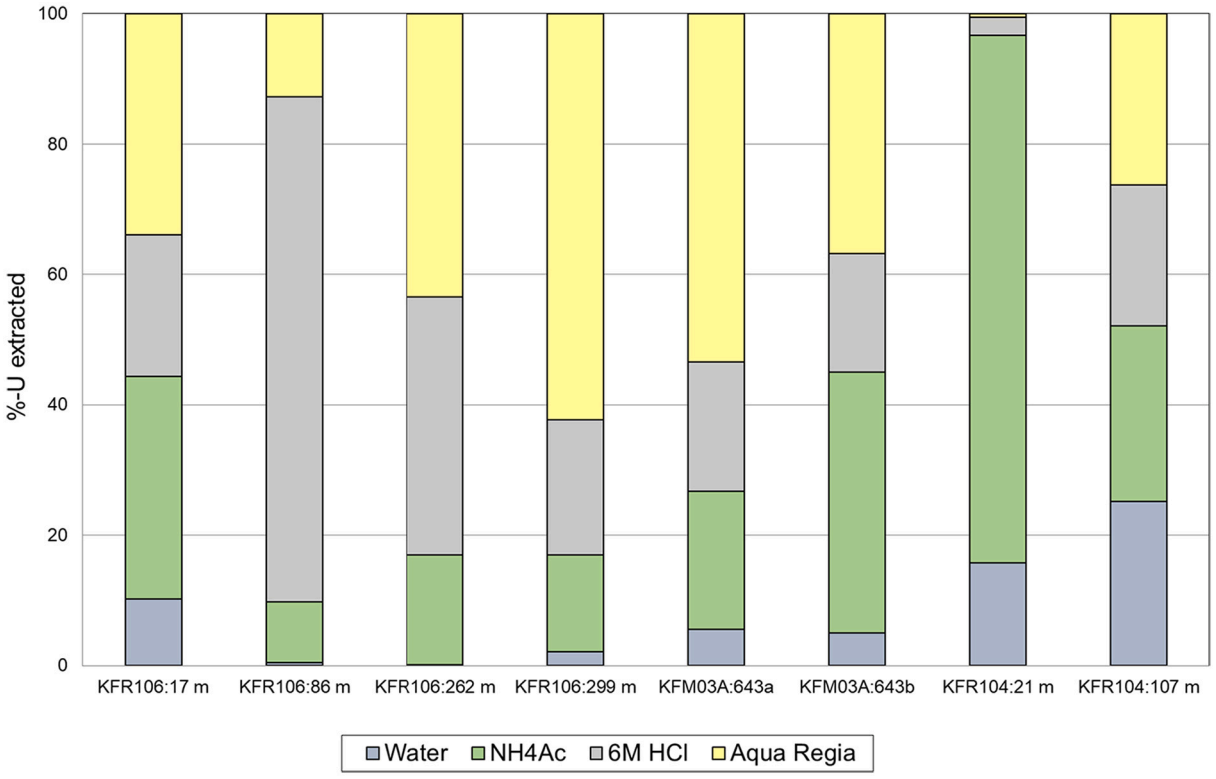

Fig. 5. Relative release of U in sequential extractions (cf. SM Table B1). Water refers to TW (Section 3.2.1).

Table 2
Comparison of U and $^{234}U/^{238}U$ AR results from tap water (TW) and synthetic groundwater (SGW) extractions. Four aliquots from the same fracture coating are measured. (1) refers to MC-ICP-MS and (2) to alpha-spectrometry, see SM Table B1). AqRg refers to bulk (whole coating material) results (*Aqua Regia* extraction). Standard deviation is given as ±2σ, – value could not be determined).

KFR106 [m]	Treatment method	U [ppm]	± σ	$^{234}U/^{238}U$	± σ	U extracted [%]
17	AqRg 1	47.6	0.07	0.946	0.005	–
	AqRg 2	58.4	1.2	0.887	0.023	–
	SGW 1	8.6	0.3	1.120	0.004	18.0
	TW 2	6.7	0.4	1.053	0.027	10.2
86	AqRg 1	129	0.07	0.918	0.003	–
	AqRg 2	142	1	0.849	0.017	–
	SGW 1	2.3	0.03	2.06	0.02	1.8
	TW 2	0.66	0.1	1.89	0.17	0.5
262	AqRg 1	3.4	0.1	1.530	0.001	–
	AqRg 2	0.9	–	1.24	0.04	–
	SGW 1	0.24	0.02	2.64	0.01	7.04
	TW 2	0.002	–	1.91	0.01	0.11
299	AqRg 1	22.7	0.2	0.865	0.002	–
	AqRg 2	19.3	0.8	0.884	0.022	–
	SGW 1	2.2	0.1	1.510	0.006	9.9
	TW 2	0.41	–	1.600	0.005	2.2

coincide with the groundwater section KFM02A:490–518 m. Water leachates from sample KFR106:299 m showed also ARs in good agreement (1.5 to 1.6), a ratio similar to the studied section KFM03A: 633–650 m. In sample KFR106:262 the ARs varied (TW AR = 1.9 and SGW AR = 2.64), where the SGW result was similar to that of the NH_4Ac extraction (AR = 2.65) (see SM Table B1). Also, the extracted amounts of U were similar. Differences in TW and SGW extraction can be due to different selectivity of the waters towards U-phases.

U-series isotopes were also analysed from the other leaching steps (SM Table B1). Sample-specific $^{234}U/^{238}U$ ARs across the leachates varied significantly, with the highest ARs in the water and NH_4Ac leachates. It is unlikely that the extractions would have caused U isotope fractionation, so the distinct $^{234}U/^{238}U$ ARs reflect dissolution of different U phases. Presence of distinct U phases is also supported by variation in the $^{230}Th/^{238}U$ and $^{230}Th/^{234}U$.

Residual material from the three extraction steps was treated in hot *Aqua Regia*. This extraction revealed a large surplus of ^{234}U and ^{230}Th in sample KFR104:21 m ($^{234}U/^{238}U$ = 3.46 and $^{230}Th/^{238}U$ = 7.74). This surplus probably formed though α-recoil of daughter isotopes, propelled into the rock matrix from U-rich phases covering the residual minerals. This is supported by the high total U in this fracture coating (over 4500 ppm). If the U-rich phase is the reason for the ^{234}U and ^{230}Th surplus, then the magnitude of the excess is proportional to the timing of U deposition, as demonstrated by Suksi and Rasilainen (1996).

4.2.2. *Distribution of U(IV) and U(VI)*

Three fracture coating samples from KFR 106 were subject to oxidation state analysis with a wet chemistry method (cf. Section 3.2.2). The U(VI) varied from 22% to 45% between the analysed samples (Table 3). The $^{234}U/^{238}U$ AR in the U(VI) fraction was systematically higher than in the U(IV) fraction, consistent with the theory that the chain decay product ^{234}U occurs more frequently in the hexavalent state and, therefore, is more leachable (Rössler, 1983; Petit et al., 1985; Adloff and Rössler, 1991; Suksi and Rasilainen, 2002). U(VI) and the $^{234}U/^{238}U$ ARs extracted by this method were similar to the total U dissolved by the water and NH_4Ac extractions for samples KFR106:17 m and KFR106:299 m. However, in KFR106:86 m, extracted U(VI) (24%) was higher than that dissolved by the water and NH_4Ac extractions (10%; Table 3). Here, a fraction of U(VI) may reside in a less soluble matrix, such as the U(IV)-bearing U-phosphate or P-rich U-silicate phase observed in the SEM study (Sandström et al., 2011). More sensitive μ-PXRD analysis was applied to identify specific U phases (SM Fig. B1.), but U concentrations were too low to determine the mineralogy (142 ppm). Nevertheless, the ~10 wt% U that is selectively removed by leaching with TW/SGW and NH_4Ac (Table 3 and Fig. 5) in the

Table 3
U(IV) and U(VI) fractions dissolved in anoxic HCl extraction. Insoluble portion of U (U_{res}) was considered U(IV). Dissolved U(VI) is compared to readily soluble U, i.e., water and NH_4Ac extracted U (cf. Fig. 5). Main minerals of fractures coatings from Sandström et al., 2011 (ad = adularia, ca = calcite, py = pyrite, chl = chlorite, qz = quartz, corr = corrensite, clay = illite-smectite, hm = hematite). *ocular mapping.

KFR106 [m] composition	U form	U [ppm]	± σ	$^{234}U/^{238}U$	± σ	U(VI) [%]	Water + NH_4Ac [%]
17	U(IV)	3.27	0.10	0.99	0.04	–	–
	U(VI)	24.6	0.5	1.12	0.02	45	44
	U_{res}	27.4	0.9	0.654	0.023	–	–
ad, ca, clay py	$U(IV)_{tot}$	30.6	–	–	–	–	–
86	U(IV)	35	1	0.806	0.018	–	–
	U(VI)	29.4	0.8	1.70	0.06	24	10
	U_{res}	60	2	0.611	0.023	–	–
ca, qz. ad, py, clay	$U(IV)_{tot}$	94	4	–	–	–	–
299	U(IV)	0.37	0.04	0.656	0.058	–	–
	U(VI)	5.13	0.17	1.37	0.04	22	17
	U_{res}	18	2	0.69	0.02	–	–
*chl, corr, ad, hm	$U(IV)_{tot}$	18.4	0.1	–	–	–	–

KFR106:86 m sample is most probably U(VI).

Uranium redox state in KFR106:86 m was also studied using the U L_3 edge HERFD-XANES spectroscopy (Fig. 6a). The HERFD spectrum exhibits several spectral features resembling those in the spectrum of U_4O_9 (marked as A, B and C). Based on a linear combination fit (LCF) analysis of the HERFD spectrum, 80% of the solid-phase U is present in mixed-valence phase (stoichiometry similar to U_4O_9) and the remaining ~20% as a U(VI) phase, such as sodium boltwoodite (Fig. 6b). The finding of a significant portion of U(VI) agrees well with the oxidation state results obtained from the wet chemistry approach where ca. 24% U (VI) was determined (see Table 3). However, in the SE experiment most U was extracted by 6 M HCl in the KFR106:86 m sample (see Section 4.2.1 and Fig. 5), which could occur as mixed-valence UO_{2+x} species, as supported by XAS measurements. Less than 15 wt% of the total U is left in the residue and refers to sparingly soluble U(IV) phases.

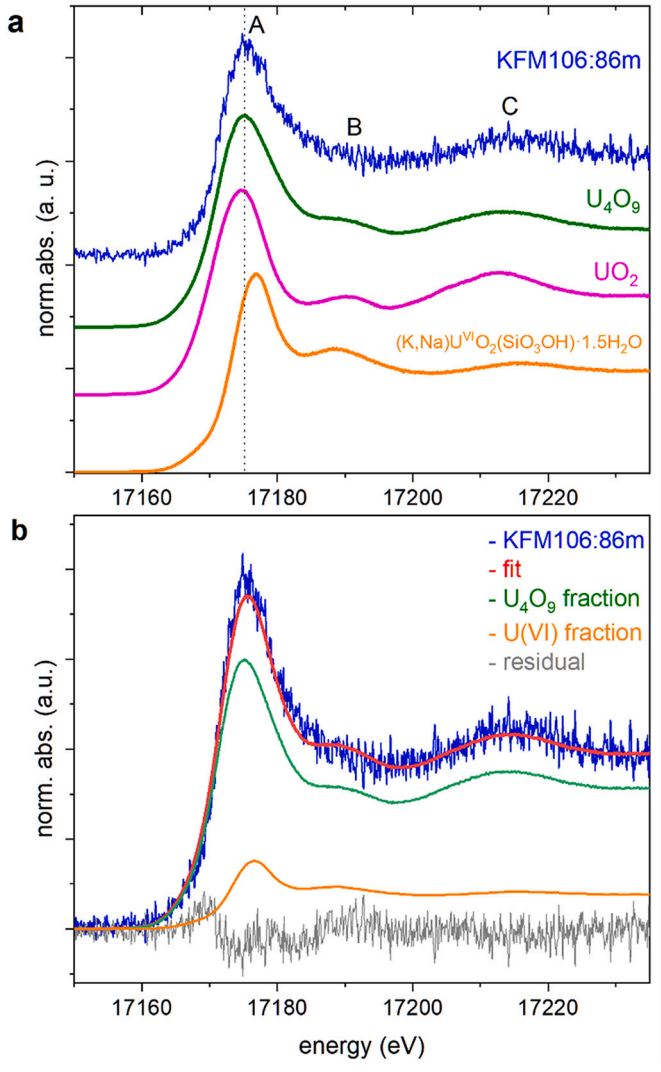

Fig. 6. U L_3 edge HERFD-XANES spectra of KFR106:86 m, U_4O_9, UO_2 and (K, Na)$UO_2(SiO_3OH)\cdot 1.5H_2O$ (boltwoodite) (**a**); LCF analysis of KFR106:86 m spectrum performed in ATHENA program shows 80% of U_4O_9 and ca. 20% of U (VI) fraction, as uranyl species (**b**).

4.3. USD results in bulk fracture coating material

Radioactive disequilibrium in the ^{238}U decay chain has been widely used to understand U mobility during water-rock interaction (e.g., Rosholt, 1983; Ivanovich and Harmon, 1992; Bourdon et al., 2003; Paces et al., 2013). In brief, disequilibrium originates from nuclear chemical processes during decay of ^{238}U and its daughters and is increased and modified by preferential mobilisation of ^{234}U relative to ^{238}U, and U relative to ^{230}Th. Recent mobility of U is recognized if α-activity ratios (AR) of the ^{238}U decay chain's longest-lived isotopes (^{238}U, ^{230}Th and ^{234}U) deviate significantly from one. The nature of U mobility has traditionally been interpreted from measured ARs plotted on a disequilibrium diagram (Fig. 7). The half-lives of ^{234}U (245 ka) and ^{230}Th (75.2 ka) are ideal to study the mobility of U within the last 150 ka. Since Th is considered immobile (cf. Langmuir and Herman, 1980) mobility of U isotopes relative to ^{230}Th can be recognized in the diagram.

In this study, USD was used to identify fractures and depths that have experienced U mobilisation or deposition within the past 150 ka. Interpretation of ARs in material sampled from open, water-conducting fractures can be challenging because disequilibrium signature is integrated over a long history of U mobility, starting from current water-rock interaction and extending to beyond the USD time scales (> 1 Ma). Fig. 8 presents ARs from Forsmark (this study) together with several study sites in the Fennoscandian shield (Blomqvist et al., 2000; Tullborg et al., 2004; Drake and Tullborg, 2008). At all sites, recent U mobility is apparent at considerable depths (several hundred meters), which can be explained by palaeohydrological similarities between the sites, with periodic intrusion of distinct waters during the last 120 ka.

ARs for most Forsmark samples (red dots) indicate U gain, i.e., U addition has controlled overall U mobility (SM Table B2). Several samples plot below the $^{234}U/^{238}U$ AR = 1 line and left of the ^{230}Th—^{234}U equiline, which indicates selective loss of ^{234}U ($^{234}U/^{238}U$ AR < 1) but also recent addition of U ($^{230}Th/^{238}U$ AR < 1) which is due to relative quantities of leached versus deposited U. This isotopic composition is possible in fractures that have been leached by groundwater over a long

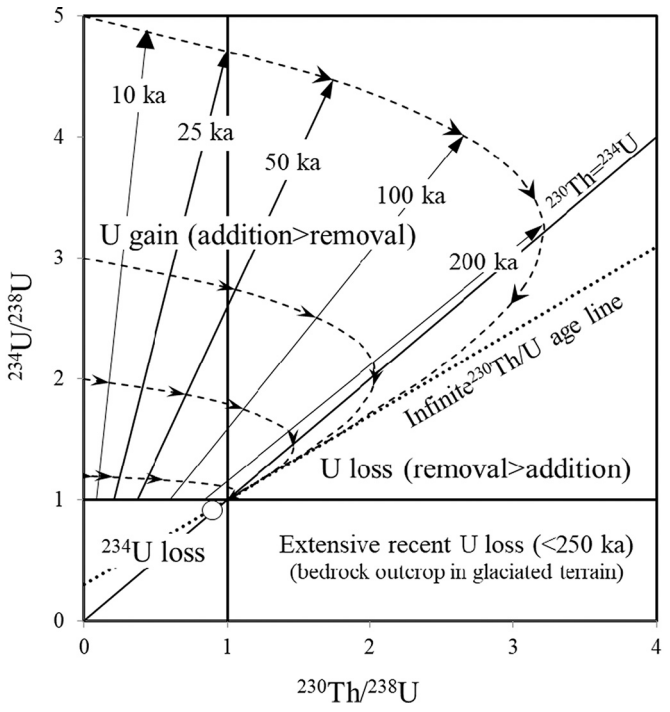

Fig. 7. U-series isotope evolution diagram showing how ^{230}Th-^{234}U-^{238}U isotope compositions can be affected by different open-system processes, including radioactive decay and secondary U mobility. Evolution of isotope composition after a sudden addition of U in a closed-system, towards infinite ^{230}Th/U age line, is also shown (isochrons after 200 ka have not been drawn here). The graph has been modified from Thiel et al. (1983), Osmond et al. (1983), and Rosholt (1983).

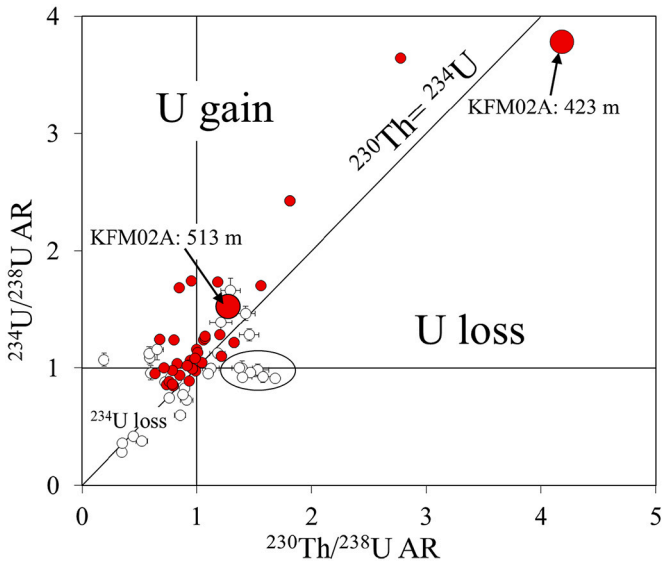

Fig. 8. U-series isotopic compositions in fracture-surface samples from Forsmark indicated in red (cf. Table 1). The two samples indicated are from fractures located in deep groundwater sections with elevated U concentrations. For comparison results from other sites in the Fennoscandian Shield (white) have been presented (collected from Blomqvist et al., 2000; Tullborg et al., 2004; Drake and Tullborg, 2008; Drake et al., 2009). Circled samples are from bedrock outcrops located in Finland on the coast of Gulf of Bothnia. (For interpretation of the references to colour in this figure legend, the reader is referred to the web version of this article.)

time period, with preferential leaching of ^{234}U. In U-gain samples (^{234}U/^{238}U AR > 1), the timing of U additions equates to the late Quaternary, because an older deposition would experience decay of excess ^{234}U and convergence of ^{234}U/^{238}U AR towards one. Several samples are at or close to equilibrium. This may be due to lack of redistribution or to a very small portion of mobile U in these fractures.

5. Discussion

The purpose of collecting experimental data was to evaluate formation pathways for the unusual U enrichment observed in the deep anoxic groundwater. Since this finding has been linked to glaciation-deglaciation water intrusions (Smellie et al., 2008), the recent mobility of sources for U were in focus. The last two water intrusions occurred as late as 18,000–11,000 y and ~7000 y ago. Their impact on U mobility should be detectable in the ^{230}Th-^{234}U-^{238}U isotope composition of the fracture-borne U source.

5.1. Uranium isotope dynamics in the deep groundwater sections

The balance between preferential release of ^{234}U and congruent dissolution of U determines the overall ^{234}U/^{238}U AR of the water. The primordial isotope ^{238}U is released through chemical processes only, whereas release of ^{234}U, being decay product of ^{238}U, can be enhanced relative to its parent through both chemical and physical processes. Preferential leaching of ^{234}U is a well-known phenomenon and explains ^{234}U excess in groundwaters. Significant preferential release of ^{234}U is possible due to its chain decay-induced auto-oxidation which makes it more susceptible to groundwater leaching (cf. Rössler, 1983; Petit et al., 1985; Adloff and Rössler, 1991; Suksi and Rasilainen, 2002). Physical release via α-recoil of the short-lived precursor ^{234}Th is an ongoing process but becomes important when the fracture surface is rich in U, water exchange is slow (on the order of ^{234}U half-life), and congruent dissolution of U does not occur.

Within the last 400 ka, the water intrusion associated with the most recent glaciations in Northern Europe, Saale and Weichsel, has strongly influenced groundwater exchange and groundwater chemistry in the upper 300 m of bedrock and to at least 1000 m depth in some fracture zones. In the groundwater section KFM02A:490–518 m, where the highest U concentrations are measured, water exchange within the last 8 ka is apparent from an analysis of non-steady state ^{223}Ra/^{226}Ra ARs (Krall et al., 2020). The large variation in U concentration (69–172 μg/L) with invariable ^{234}U/^{238}U AR found during several consecutive years of monitoring this groundwater offered a unique tool to evaluate the U source. Variation in the U concentration during the monitoring is not clear but might be due to disturbances in flow conditions introduced by the drilling activities and subsequently by the sampling itself (Nilsson et al., 2020).

In the groundwater sections KFM02A:490–518 m and KFM03A:633–650 m, the ^{234}U/^{238}U ARs revealed congruent dissolution of a U source that has the same ^{234}U/^{238}U AR as the respective waters (cf. Section 4.1). Here, high groundwater U concentrations point to a readily soluble U(VI) source, as corroborated by the speciation-solubility calculations performed for KFM02A:490–518 m (Tullborg et al., 2017 and references therein). Since ^{234}U/^{238}U ARs are clearly over one (i.e., excess ^{234}U has not fully decayed), the U source phase likely accumulated during the late Quaternary and has since participated in U mass exchange during U redistribution.

The groundwater section KFM02A:411–442 m, on the other hand, yielded a ^{234}U/^{238}U release ratio that was smaller than the ^{234}U/^{238}U AR of the respective water (2.05 and 3.5, respectively; Fig. 4). Furthermore, the ^{234}U—^{238}U correlation trend line did not intercept origin but rather the positive y-axis (Fig. 4). This finding suggests the involvement of more than one U source, one that supplied U to the water at the AR of ~2 and another that supplied excess ^{234}U. A source for ^{234}U could be an old U(IV)-rich phase, such as the secondary uraninite or the metamict

uranothorite found in local pegmatites (Krall et al., 2015). The other source is evidently a U(VI) phase from which U has congruently dissolved at an AR of ~2, possibly the same source as for section KFM02A:490–518 m (Fig. 8).

The persistence of high U concentrations in the section KFM02A:490–518 m several thousand years after the last water intrusion (brackish marine water) implies that the geochemical constituents of the groundwater can stabilise dissolved U, thereby inhibiting significant U deposition despite the anoxic conditions. Nevertheless, some deposition may have occurred, and this possibility was addressed in the simulations (Chapter 6). Interestingly, the modelling discussed in Krall et al. (2020) also indicates that simultaneous dissolution of U(VI)-phase and reprecipitation of U(IV)-oxide is thermodynamically feasible in KFM02A:490–518 m.

The possibility that the brackish Littorina Seawater, itself, transported U-rich water into the deep bedrock aquifer was excluded because both high and low U concentrations have been measured in this water-type throughout the site without significant changes in the overall groundwater chemistry. Instead, the groundwater remobilised U that was previously deposited in the fracture network (cf. Sandström et al., 2008; Krall et al., 2015; Tullborg et al., 2017; Krall et al., 2020). The identification of the $Ca_2UO_2(CO_3)_3^0$ complex in the groundwater with the highest dissolved U corroborates this interpretation (cf. Tullborg et al., 2017).

5.2. Uranium mobility in fracture coatings

Large changes in flow conditions during the last glacial cycle left Forsmark groundwater chemistry in transient state. Consequently, steady-state conditions in U-series isotopes on fracture surfaces would not be expected in conductive fractures shallower than 800 m. This reflected by the range of disequilibrium ARs, recording both U gain and ^{234}U loss throughout the fracture network. ^{234}U loss was principally indicated in fracture coatings from shallow depths (upper 115 m), where differences in the character of recharging waters can drive intense U leaching. Leaching of U along near-surface fractures and extending centimetres into the rock matrix was reported from the Palmottu natural analogue study site in southern Finland (cf. Rasilainen et al., 2003). Generally, ^{234}U deficiency ($^{234}U/^{238}U < 1$) on fracture surfaces also reflects long-term chemical stability of the U source in the host phase.

Most mineral coatings in the presently water-conducting fractures are of hydrothermal origin and Palaeozoic or Precambrian in age (Sandström et al., 2009). Flow routes at the site have varied over time, in connection to changes in hydraulic pressure and surface hydrogeology (cf. Follin et al., 2007, 2008). No correlation was found between disequilibrium isotopic composition and fracture transmissivity (water flow m^2/s). Instead, samples from borehole sections with no measurable transmissivity showed disequilibrium (white dots in Fig. 9). Near-term hydraulic isolation can be explained by the post-glacial unloading of the site, which has reduced fracture transmissivity or disconnected fractures from the main flow. Findings of pockets with high portions of dilute glacial meltwater at depth of 200 to 400 m (Nilsson et al., 2011) support this interpretation.

Information obtained from the sample KFM02A:513 m, located in the groundwater section with highest U, indicate U gain ($^{234}U/^{238}U = 1.18$ and $^{230}Th/^{238}U = 1.53$) and, as such, does not indicate that the analysed fracture surface has supplied U to the groundwater. Although U dissolution may have occurred, overall addition of U masks the signature. This possibility was addressed in numerical simulations (Section 6). ARs of sample KFM02A:423 m, situated 100 m above sample KFM02A:513 m, indicate the opposite scenario, with loss of U ($^{230}Th/^{234}U = 1.1$) with minor and recent U addition ($^{234}U/^{238}U = 3.78$) (see Fig. 8).

The SE study revealed that coating material contains both weakly and more tightly bound U. The fraction of easily extractable U, considered to be U(VI), varied between samples. This is consistent with determinations of U redox state, which showed analogous variation in

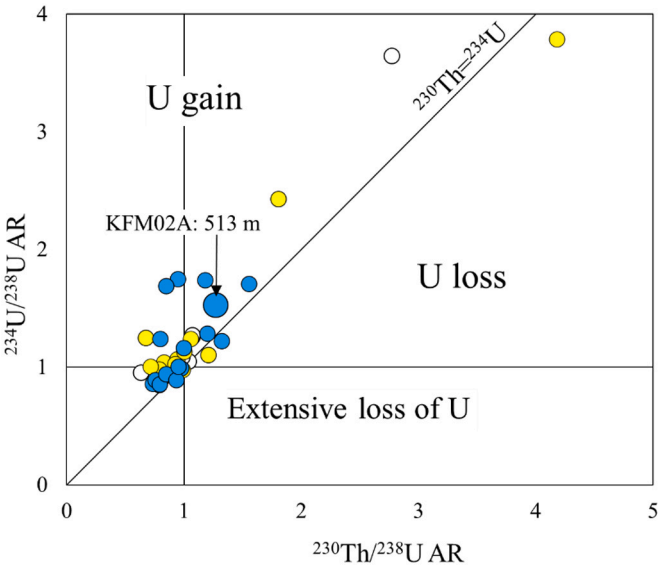

Fig. 9. U-series isotopic composition and fracture transmissivities. Blue: most transmissive, 10^{-7}-10^{-5} m^2/s, yellow: 10^{-11} to 10^{-8} m^2/s and white: no measurable transmissivity. The sample from the highest U groundwater section is indicated. (For interpretation of the references to colour in this figure legend, the reader is referred to the web version of this article.)

dissolved U(IV) and U(VI) phases (cf. Section 4.2.2; Table 3). The U(VI) fraction separated by the anoxic 4.5 M HCl extraction was similar or larger than the U fraction determined for the water+NH_4Ac leachate in all three samples studied. In KFR106:86 m U(VI) clearly exceeds the easily dissolvable fraction. In this sample the redox state was also determined by the U L_3 edge HERFD-XANES technique. This method gave similar redox state information and showed the presence of a mixed-valence U mineral, possibly the UO_{2+x} and/or P-rich U-silicate phase observed in the SEM study (Sandström et al., 2011). A previous study by Pidchenko et al. (2013) likewise showed that carefully designed chemical extraction in geological sample material gives U(IV)/U(VI) results that agree well with instrumental methods.

The $^{234}U/^{238}U$ ARs in the U(VI) fraction and in the easily extractable U fraction (water+NH_4Ac) agreed for samples KFR106:17 m and KFR106:299 m demonstrating that U(VI) is hosted in easily dissolvable phases in these samples. In contrast, in sample KFR106:86 m the $^{234}U/^{238}U$ ARs were different in U(VI) fraction (1.7), water leachate (1.9) and NH_4Ac leachate (1.4). This is in line with the presence of more than one distinct U(VI) phases, e.g. U co-precipitated with calcite, individual U(VI) minerals and U(VI) in stable P/Si matrix.

6. Numerical simulation of U redistribution

6.1. Description of system behaviour

The U system is situated in a fracture at ~500 m depth, where ARs on fracture surfaces have evolved through radioactive decay and through U redistribution leading to elevated U concentrations in the groundwater. The uranium source for the deep groundwater originates from U leached from the overburden and from fracture surfaces along the flow path during glacial cycles before it is gradually deposited on fracture surfaces at depth. There is strong evidence from the isotopic study (cf. Section 4.1) that ^{234}U and ^{238}U have not fractionated, so the $^{234}U/^{238}U$ AR remains unchanged during redistribution.

6.2. Simulations

In our model, U mobility parameters reflect deposition and congruent dissolution. Due to elevated U in the system, adsorption and

desorption and selective leaching of ^{234}U are less important for the overall mobility of U (cf. Section 4.2.1).

The evolution of isotopic composition is calculated by radioactive decay/in-growth equations that include a term for U input and output fluxes (cf. Azzam et al., 2009). In the simulation, the specified mobile fraction of U was based on results from the water extractions (Section 4.2.1) and was ascribed the same $^{234}U/^{238}U$ AR as measured in the groundwater (cf. Section 4.1). Since measured ARs of sample KFM02A:513 m indicated U gain, we focused the simulations on U redistribution scenarios with overall dissolution/deposition flux ratios below unity.

The isotopic composition 120 ka ago, after the Saale glaciation, is unknown and was therefore estimated. For the estimation, it was assumed that the U system evolved similarly during both glaciation cycles. Therefore, the isotopic composition after the last glaciation (Weichselian), which could be obtained from the studied fracture surface sample ("reference"), was considered a reasonable choice. Redistribution scenarios were constructed within the framework of the climate reconstruction outlined in Table 4.

The reconstruction consisted of two periods with glacial conditions, each followed by transgression of the Baltic Sea, the most recent glaciation being the most prominent (cf. Fredén, 2002; SKB, 2010, and references therein). U fluxes were transferred from the fracture surface to the groundwater during periods of brackish water intrusion, succeeded by reverse mass transfer from the groundwater to the fracture surface after the intrusion. During the brackish Littorina sea water intrusion considerable U dissolution was assumed based on groundwater chemistry. During periglacial, glacial, and permafrost periods, the system was considered non-dynamic with negligible mobility of U and U-series isotope composition evolved only by radioactive decay. Input parameters for the numerical simulation are presented in Supplementary Material (Table C1).

Table 4
Climate reconstruction for the past 120 ka (cf. SKB, 2010 report Fig. 4-22) and assumed impact on U mobility in deep groundwater environment.

Time [ka]	Climate conditions	Hydrogeological conditions	Impact at around 500 m depth
0–23	Mixed temperate and permafrost conditions	Relatively stable	Negligible or no impact.
23–38	Periglacial	Hydrogeologically stable due to permafrost	
38–42	Mixed temperate and permafrost conditions	Relatively stable	
42–62	Periglacial and glacial (basal frozen conditions)	Hydrogeologically stable due to permafrost	
62–66	Glacial (basal melting conditions)	Recharge of meltwater	Deposition
66–75	Submerged conditions (brackish sea water)	Some intrusion of brackish water due to density turnover. No indication of a high salinity in this water based on the current understanding of the groundwater evolution and therefore less driving force for density intrusion.	Dissolution due to elevated alkalinity and Ca concentration
75–90	Periglacial	Hydrogeologically stagnant due to permafrost	Negligible or no impact.
90–109	Glacial (basal melting conditions)	Recharge of meltwater	Deposition.
109–115	Submerged conditions (first fresh water (Ancylus Lake and thereafter Brackish Sea water)	Intrusion due to density turnover of brackish sea water with variable salinity. The Littorina Sea maximum at about 7 ka being the most saline.	Dissolution due to high alkalinity and Ca contents. Dissolution more intense than in the period 66–75 ka. The process was most prominent during the Littorina maximum some 7 ka ago.
115–120	Temperate	Intrusion of meteoric water in the shallow bedrock. No real impact below 100 m.	Deposition

6.3. Simulation results

Numerous U redistribution scenarios were tested. Activity ratios at or close to reference were used as starting ARs and overall dissolution/deposition ratios ranging from 0.43 to 1.25 were chosen. Scenarios and simulation results are presented in SM Table C1 and plotted in Fig. 10. Reference ARs were chosen to test the hypothesis that the U system evolved similarly during both glaciation cycles. Respective scenarios yielded ARs close to reference, in support of this hypothesis. Even better agreement with the reference was obtained with a slightly higher starting $^{234}U/^{238}U$ AR (1.60–1.65) and lower starting $^{230}Th/^{234}U$-$^{230}Th/^{238}U$ ARs (0.70–0.75 and 1.15–1.2) and when overall dissolution/deposition flux ratios were set to 0.43–0.57 (circled values in Fig. 10).

It was found that if U was let to deposit after the Littorina Sea water intrusion (late Holocene) it increased the compatibility between simulation results and the reference. Increasing the flux ratio from 0.75 to 1.25 resulted in ARs that approached and crossed $^{230}Th = {}^{234}U$ equiline. Since this would reflect substantial loss of U from the system, these scenarios can be omitted. Similarly, the scenarios with no U fluxes (R0, EA0, EB0 and EC0 in Table C1) or fluxes only after the Weichselian glaciation (EA20, EB20 and EC20) can also be excluded because the simulation results significantly differed from the reference. An example of Decservis-2 graphical output of ARs' evolution over time for a viable

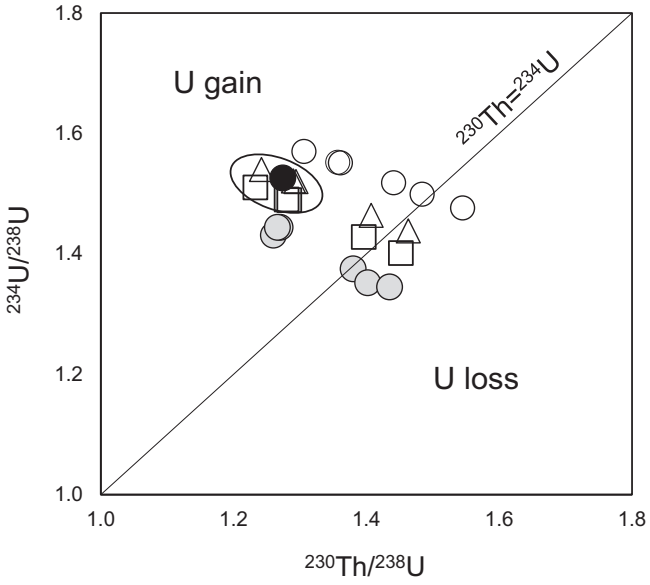

Fig. 10. Simulation results from U redistribution scenarios with different starting ARs and dissolution/deposition flux ratios. Grey circles represent scenarios starting from reference ARs (sample KFM02A:513 m). Other markers result from scenarios with slightly different starting ARs. Scattering within marker series reflect variable dissolution/deposition flux ratios (cf. SM Table C1). Good agreement with the reference (black) is obtained in scenarios with starting ARs $^{230}Th/^{238}U$ 1.15–1.20 and $^{234}U/^{238}U$ 1.60–1.65 and overall flux ratios of 0.43–0.57 (see Section 6.3).

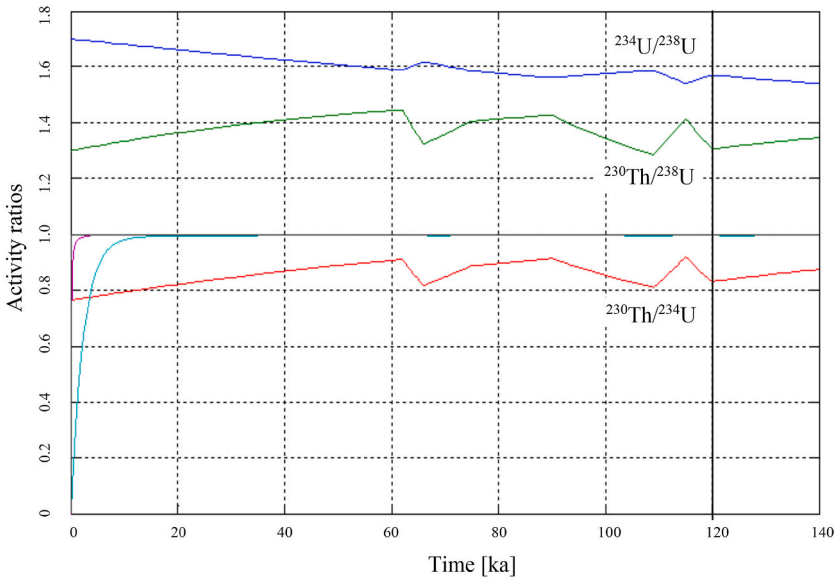

Fig. 11. Example of Decservis-2 graphical output. Evolution of ^{230}Th-^{234}U-^{238}U isotope compositions under U redistribution scenario EC1, with starting ARs ^{234}U/^{238}U = 1.7, ^{230}Th/^{238}U = 1.3 and ^{230}Th/^{234}U = 0.76. Kinks in curves refer to U dissolution and deposition. Overall U dissolution/deposition flux ratio is set to 0.43. Curves at the beginning of graph belong to the short-lived daughters and are not discussed here.

scenario is presented in Fig. 11.

Simulations could reproduce the U redistribution process that yielded disequilibrium isotopic composition in the sample KFM02A:513 m. A simple calculation shows that the simulated U fluxes are realistic: The fracture coating was gently scratched off from a surface area of about 0.008 m^2. The sample weighing 0.298 g contained 31.5 μg U/g which gives 9 μg of U and for an area of 1 m^2 1140 μg U. With 1 mm fracture aperture (cf. Forsman et al., 2004) the water volume would be 1 L. Using the water-extractable part of U (10% of total extractable U) as U dissolution flux would yield a concentration over 100 μg U/L, which is similar to the concentrations measured in groundwater section KFM02A:490–518 m. Smaller apertures (<1 mm), which are common in this drill core section, would yield much higher U concentrations which may have prevailed immediately after the Littorina Sea water intrusion. The calculation is a rough estimation, but it gives a reasonable view of U fluxes contributed to the unusually high U concentration in the groundwater.

7. Conclusions

We have investigated U redistribution in fractures to understand the reason for unusually high U concentrations in anoxic deep groundwater. The study has produced the following crucial findings:

- U mobility was identified in fractures as deep as 700 m, and it is realistic to assume that this mobility is, to large extent, related to recent water intrusions during the last glacial cycle.
- The U redistribution is broadly characterized as U gain, but some fractures, typically those located in the upper bedrock, showed a ^{234}U loss, an indicator of long-term U leaching.
- Large portions (up to 25%) of the U in fracture coatings were water-soluble and, in the more mobile U(VI) oxidation state.
- From groundwater monitoring data (at 500 to 630 m depth), we were able to identify the ^{234}U/^{238}U AR of solid-phase U that participated in the recent U redistribution.
- The findings above and relevant information from the site were used in the simulation, which could reproduce the isotopic composition in the studied fracture coating. Because the simulation included dissolution during two periods, the most recent some 7000 y ago, it is apparent that this dissolution is masked by the overall signature of deposition (U gain).

A simple mass balance calculation shows that the simulated U fluxes during U redistribution are realistic and can explain the measured high content in the anoxic groundwater at 500 m depth.

Declaration of Competing Interest

The authors declare that they have no known competing financial interests or personal relationships that could have appeared to influence the work reported in this paper.

Acknowledgement

This study has been financed by SKB (Swedish Nuclear Fuel and Waste Management Co). Ignasi Puigdomenech, SKB is thanked for support at all stages. Jens-Ove Näslund, SKB provided important guiding concerning climate scenario for the modelling. John Smellie provided knowledge about the sophisticated sampling technique and took also part in the sampling. Kent Åkerström performed careful sampling and documentation at the site. Cecilia Berg, SKB, helped with sampling in the field. Ann-Chatrin Nilsson, Geosigma AB, helped with figures and hydrogeochemical data. Lillemor Claesson-Liljedahl, SKB, provided comments improving the manuscript. Mats Tröjbom helped with the groundwater data and supply of plots. Yann Lahaye, Geological Survey of Finland, is acknowledged for guidance in MC-ICP-MS. Two anonymous reviewers are acknowledged for constructive technical review and usefull suggestions.

Appendix A. Supplementary data

Supplementary data to this article can be found online at https://doi.org/10.1016/j.chemgeo.2021.120551.

References

Adloff, J.P., Rössler, K., 1991. Recoil and transmutation effects in the migration behavior of actinides. Radiochim. Acta 52/53, 269–274. https://doi.org/10.1524/ract.1991.5253.1.269.

Azzam, S., Suksi, J., Ammann, M., 2009. DECSERVIS-2: a tool for natural decay series mass flow simulation. Appl. Radiat. Isot. 67, 1992–1997. https://doi.org/10.1016/j.apradiso.2009.07.021.

Bernhard, G., Geipel, G., Reich, T., Brendler, V., Amayri, S., Nitsche, H., 2001. Uranyl(VI) carbonate complex formation: validation of the $Ca_2UO_2(CO_3)_3$ (aq) species. Radiocheim. Acta 89, 511–518. https://doi.org/10.1524/ract.2001.89.8.511.

Blomqvist, R., Ruskeeniemi, T., Kaija, J., Ahonen, L., Paananen, M., Smellie, J.T.A., Grundfelt, B., Pedersen, K., Bruno, J., Pérez del Villar, L., Cera, E., Rasilainen, K., Pitkänen, P., Suksi, J., Casanova, J., Read, D., Frape, S., 2000. The Palmottu natural Analogue Project – Phase II: Transport of radionuclides in a natural flow system at Palmottu. In: European Commission. Report EUR 19611 EN, 171 p. + 1 Appendix.

Bolle, J.N., Martin, H., Sondag, F., Cardoso Fonseca, E., 1988. Selective chemical extraction of uranium from mineral, soil and stream sediment samples at Horta da Vilariça, Northeastern Portugal. Uranium 4, 327–340.

Bourdon, B., Henderson, G.M., Lundstrom, C.C., Turner, S.P., 2003. Uranium-Series Geochemistry, Reviews in Mineralogy & Geochemistry, Vol. 52, p. 656.

Cederbom, C., Larson, S.Å., Tullborg, E.-L., Stiberg, J.-P., 2000. Fission track thermochronology applied to Phanerozoic thermotectonic events in central and southern Sweden. Tectonophysics 316, 153–167. https://doi.org/10.1016/s0040-1951(99)00230-9.

Chabaux, F., Bourdon, B., Riotte, J., 2008. Review of models for U-series fractionation in surficial environments. In: Krishnaswami, S., Cochran, J.K. (Eds.), Radioactivity in the Environment, U-Th Series Nuclides in Aquatic Systems. Elsevier, pp. 81–86.

Drake, H., Tullborg, E.-L., 2008. Fracture mineralogy Laxemar. In: Site Descriptive Modelling SDM-Site Laxemar. SKB Report R-08-99. Swedish Nuclear Fuel and Waste Management Co. Stockholm, Sweden.

Drake, H., Tullborg, E.-L., Mackenzie, A.B., 2009. Detecting the near-surface redox front in crystalline bedrock using fracture mineral distribution, geochemistry and U-series disequilibrium. Appl. Geochem. 24, 1023–1039. https://doi.org/10.1016/j.apgeochem.2009.03.004.

Drake, H., Heim, C., Roberts, N.M.W., Zack, T., Tillberg, M., Whitehouse, M., Broman, C., Ivarsson, M., Whitehouse, M., Åström, M., 2017. Isotopic evidence for microbial production and consumption of methane in the upper continental crust throughout the Phanerozoic eon. Earth Planet. Sci. Lett. 470, 108–118. https://doi.org/10.1016/j.epsl.2017.04.034.

Follin, S., Levén, J., Hartley, L., Jackson, P., Joyce, S., Roberts, D., Swift, B., 2007. Hydrogeological Characterisation and Modelling of Deformation Zones and Fracture Domains, Forsmark Modelling Stage 2.2. SKB report R-07-48. Swedish Nuclear Fuel and Waste Management Co. Stockholm, Sweden.

Follin, S., Stephens, M.B., Laaksoharju, M., Nilsson, A.-C., Smellie, J.A.T., Tullborg, E.-L., 2008. Modelling the evolution of hydrochemical conditions in the Fennoscandian Shield during Holocene time using multidisciplinary information. Appl. Geochem. 23, 2004–2020. https://doi.org/10.1016/j.apgeochem.2008.02.022.

Forsman, I., Zetterlund, M., Rhén, I., 2004. Correlation of Posiva Flow Log anomalies to core mapped features in Forsmark (KFM1A to KFM05A). In: SKB Report R-04-77. Swedish Nuclear Fuel and Waste Management Co., Stockholm, Sweden.

Fredén, C., 2002. Berg och Jord. In: Sveriges Nationalatlas, 3rd edition. Förlag, SNA. ISBN 91-87760-27-4.

Gascoyne, M., 1997. Evolution of redox conditions and groundwater composition in recharge-discharge environments on the Canadian Shield. Hydrogeol. J. 5, 4–18. https://doi.org/10.1007/s100400050253.

Geckeis, H., Lutzenkirchen, J., Polly, R., Rabung, T., Schmidt, M., 2013. Mineral-water interface reactions of actinides. Chem. Rev. 113, 1016–1062. https://doi.org/10.1021/cr300370h.

Glatzel, P., Bergmann, U., 2005. High resolution 1s core hole X-ray spectroscopy in 3d transition metal complexes – electronic and structural information. Coord. Chem. Rev. 249, 65–95. https://doi.org/10.1016/j.ccr.2004.04.011.

Goettlicher, J., Kotelnikov, A., Suk, N., Kovalski, A., Vitova, T., Steininger, R., 2013. Sulfur K X-ray absorption near edge structure spectroscopy on the photochrome sodalite variety hackmanite. Zeitschrift für Kristallographie - Crystal. Mater. 228, 157–171.

Hammersley, A.P., Svensson, S.O., Hanfland, M., Fitch, A.N., Häusermann, D., 1996. Two-dimensional detector software: from real detector to idealised image or two-theta scan. High Pressure Res. 14, 235–248.

Ivanovich, M., Harmon, R.S., 1992. Uranium-Series Disequilibrium, Applications to Earth, Marine, and Environmental Sciences, , 2nd ed1992. Clarendon Press, Oxford, p. 910.

Krall, L., Sandström, B., Tullborg, E.-L., Evins, L.Z., 2015. Natural uranium in Forsmark, Sweden: the solid phase. Appl. Geochem. 59, 178–188. https://doi.org/10.1016/j.apgeochem.2015.04.020.

Krall, L., Evins, L.Z., Kooijman, E., Whitehouse, M., Tullborg, E.-L., 2019. Tracing the paleoredox conditions at Forsmark, Sweden, using uranium mineral geochronology. Chem. Geol. 506, 68–78. https://doi.org/10.1016/j.chemgeo.2018.12.013.

Krall, L., Auqué-Sanz, L., Garcia-Orellana, J., Trezzi, G., Tullborg, E.-L., Suksi, J., Porcelli, D., Andersson, P., 2020. Radium isotopes to trace uranium redox anomalies in anoxic groundwater. Chem. Geol. 531 https://doi.org/10.1016/j.chemgeo.2019.1192926.

Laaksoharju, M., Smellie, J., Tullborg, E.-L., Gimeno, M., Hallbeck, L., Molinero, J., Waber, N., 2008. Bedrock hydrogeochemistry Forsmark. In: Site Descriptive Modelling SDM-Site SKB Report R-08-47. Swedish Nuclear Fuel and Waste Management Co., Stockholm, Sweden.

Laaksoharju, M., Smellie, J., Tullborg, E.-L., Wallin, B., Drake, H., Gascoyne, M., Gimeno, M., Gurban, I., Hallbeck, L., Molinero, J., Nilsson, A.-Ch., Waber, N., 2009. Bedrock hydrogeochemistry Laxemar. In: Site Descriptive Modeling SDM-Site Laxemar. SKB report R-08-93. Swedish Nuclear Fuel and Waste Management Co. Stockholm, Sweden.

Langmuir, D., Herman, J.S., 1980. The mobility of thorium in natural waters at low temperatures. Geochim. Cosmochim. Acta 44, 1753–1766.

Löfvendahl, R., Holm, E., 1981. Radioactive disequilibria and apparent ages of secondary uranium minerals from Sweden. Lithos 14, 189–201.

Luo, X., Rehkämper, M., Lee, D.-C., Halliday, A.N., 1997. High precision $^{230}Th/^{232}Th$ and 234U/238U measurements using energy-filtered ICP magnetic sector multiple collector mass spectrometry. Int. J. Mass Spectrom. Ion Process. 171, 105–117.

Näslund, J.-O., 2010. Climate and climate-related issues for the safety assessment SR-Site. In: SKB technical report TR 10-49. Swedish Nuclear Fuel and Waste Management Co, Stockholm, Sweden, p. 328.

Nilsson, A.-C., Tullborg, E.-L., Smellie, J., Gimeno, M., Gómez, J.B., Auqué, L.F., Sandström, B., Pedersen, K., 2011. SFR site investigation. In: Bedrock Hydrogeochemistry SKB Report R-11-06. Swedish Nuclear Fuel and Waste Management Co., Stockholm, Sweden.

Nilsson, A.-C., Gimeno, M.J., Tullborg, E.-L., Smellie, J., Jönsson, S., Puigdomenech, I., Berg, C., 2020. Review article methodology for hydrogeochemical sampling to characterise groundwaters in crystalline bedrock: developments made within the swedish radwaste programme. Geofluids. https://doi.org/10.1155/2020/8740492. Article ID 8740492.

Osmond, J.K., Cowart, J.B., Ivanovich, M., 1983. Uranium isotopic disequilibrium in ground water as an indicator of anomalies. Int. J. Appl. Radiat. Isot. 34, 283–308. https://doi.org/10.1016/B978-0-08-029158-1.50026-X.

Paces, J.B., Nichols, P.J., Neymark, L.A., Rajaram, H., 2013. Evaluation of Pleistocene groundwater flow through fractured tuffs using a U-series disequilibrium approach, Pahute Mesa, Nevada, USA. Chem. Geol. 358, 101–118.

Petit, J.-C., Langevin, Y., Dran, J.-C., 1985. U-234/U-238 disequilibrium in nature: theoretical reassessment of the various proposed models. Bull. Mineral. 108, 745–753.

Pidchenko, I., Salminen-Paatero, S., Rothe, J., Suksi, J., 2013. Study of uranium oxidation states in geological material. J. Environ. Radioact. 124, 141–146. https://doi.org/10.1016/j.jenvrad.2013.04.008.

Pidchenko, I., Kvashnina, K.O., Yokosawa, T., Rossberg, A., Finck, N., Schild, D., Bahl, S., Bohnert, E., Dardenne, K., Rothe, J., Schäfer, T., Geckeis, H., Vitova, T., 2017. Uranium redox transformations after U(VI) coprecipitation with magnetite nanoparticles. Environ. Sci. Technol. 51 (4), 2217–2225. https://doi.org/10.1021/acs.est.6b04035.

Posiva 2011–02, 2011. Olkiluoto Site Description 2011, Part 2. Posiva Oy, Eurajoki, Finland.

Rasilainen, K., Suksi, J., Ruskeeniemi, T., Pitkänen, P., Poteri, A., 2003. Release of uranium from rock matrix—a record of glacial meltwater intrusions? J. Contam. Hydrol. 61, 235–246.

Rauret, G., Quevauviller, Ph., 1992. Proceedings of the Workshop on the sequential extraction of trace metals in soils and sediments. Int. J. Environ. Anal. Chem. 51, 235.

Ravel, B., Newville, M., 2005. ATHENA, ARTEMIS, HEPHAESTUS: data analysis for X-ray absorption spectroscopy using IFEFFIT. J. Synchrotron Radiat. 12, 537–541. https://doi.org/10.1107/S0909049505012719.

Read, D., Black, S., Buckby, T., Hellmuth, K.-H., Marcos, N., Siitari-Kauppi, M., 2008. Secondary uranium mineralization in southern Finland and its relationship to recent glacial events. Glob. Planet. Chang. 60, 235–249.

Rosholt, J.N., 1983. Isotopic composition of uranium and thorium in crystalline rocks. J. Geophys. Res. 88, 7315–7330. https://doi.org/10.1029/JB088iB09p07315.

Rössler, K., 1983. Uranium recoil reactions. In: Gmelin Handbook of Inorganic Chemistry, 8th ed. Springer-Verlag, Berlin, pp. 135–164. Uranium, Supplement Volume A6.

Rothe, J., Altmaier, M., Dagan, R., Dardenne, K., Fellhauer, D., Gaona, X., González-Robles, E., Herm, M., Kvashnina, K., Metz, V., Pidchenko, I., Schild, D., Vitova, T., Geckeis, H., 2019. Fifteen years of radionuclide research at the KIT synchrotron source in the context of the nuclear waste disposal safety case. Geosciences 9, 2–91.

Sandström, B., Tullborg, E.-L., Smellie, J., MacKenzie, A., Suksi, J., 2008. SKB Report R-08-102. Swedish Nuclear Fuel and Waste Management Co. Stockholm, Sweden.

Sandström, B., Tullborg, E.-L., Larson, S.Å., Page, L., 2009. Brittle tectonothermal evolution in the central Fennoscandian Shield as recorded by paragenesis, orientation and $^{40}Ar/^{39}Ar$ geochronology of fracture minerals at Forsmark, Sweden. Tectonophysics 478, 158–174.

Sandström, B., Nilsson, K., Tullborg, E.-L., 2011. Site investigation SFR. In: Fracture Mineralogy Including Identification of Uranium Phases and Hydrochemical Characterisation of Groundwater in Borehole KFR106. SKB Report P-11-41. Swedish Nuclear Fuel and Waste Management Co, Stockholm, Sweden.

Sandström, B., Tullborg, E.-L., Sidborn, M., 2014. Iron hydroxide and redox capacity in bedrock fractures in the vicinity of SFR. In: SKB Report R-12-11. Swedish Nuclear Fuel and Waste Management Co., Stockholm, Sweden.

SKB, 2008. Site description of Forsmark at completion of the site investigation phase. In: SDM-Site Forsmark. SKB report TR-08-05. Swedish Nuclear Fuel and Waste Management Co, Stockholm, Sweden.

SKB, 2010. Climate and Climate-related issues for the safety assessment SR-Site. In: SKB Report TR-10-49. Swedish Nuclear Fuel and Waste Management Co, Stockholm, Sweden.

Skwarzec, B., Boryło, A., Strumińska, D.I., 2004. Activity Disequilibrium between ^{234}U and ^{238}U Isotopes in Southern Baltic. J. Radioanal. Nucl. Chem. 159 (1), 165–173. https://doi.org/10.1007/s10967-014-3001-9.

Smellie, J., Tullborg, E.-L., Nilsson, A.-C., Sandström, B., Waber, N., Gimeno, M., Gascoyne, M., 2008. Explorative analysis of major components and isotopes. In: SDM-Site Forsmark. SKB R-08-84 Swedish Nuclear Fuel and Waste Management Co, Stockholm, Sweden.

Steger, H.F., Bowman, W.S., 1980. Reference Uranium-Thorium Ore DL-1a, Certificate of Analysis, CANMET Report 80–10E. CANMET, Energy, Mines and Resources, Canada.
Stephens, M.B., 2010. Bedrock geology – overview and excursion guide. In: Forsmark Site Investigation. SKB report R-10-04. Swedish Nuclear Fuel and Waste Management Co, Stockholm, Sweden.
Stephens, M.B., Fox, A., La Pointe, P., Isaksson, H., Simeonov, A., Hermansson, K., Öhman, J., 2008. Geology forsmark. In: Site descriptive Modelling Forsmark Stage 2.2. SKB Report R-07-45. Swedish Nuclear Fuel and Waste Management Co, Stockholm, Sweden.
Suksi, J., Rasilainen, K., 1996. On the role of α-recoil in uranium migration. Radiochim. Acta 74, 297–302. https://doi.org/10.1524/ract.1996.74.special-issue.297.
Suksi, J., Rasilainen, K., 2002. Isotopic fractionation of U reflecting redox conditions around a groundwater flow route. In: Materials Research Society Symposium Proceedings, 663, pp. 961–969. https://doi.org/10.1557/PROC-663-961.
Suksi, J., Salminen, S., 2007. Study of U oxidation states in groundwater with high U concentrations. In: SKB P-07-54. Swedish Nuclear Fuel and Waste Management Co., Stockholm, Sweden.
Suksi, J., Rasilainen, K., Pitkänen, P., 2006. Variations in 234U/238U activity ratios in groundwater – a key to flow system characterisation? Phys. Chem. Earth, Parts A/B/C 31, 556–571. https://doi.org/10.1016/j.pce.2006.04.007.
Thiel, K., Vorwerk, R., Saager, R., Stupp, H.D., 1983. ^{235}U fission tracks and ^{238}U-series disequilibria as a means to study recent mobilization of uranium in Archaean pyritic conglomerates. Earth Planet. Sci. Lett. 65, 249–262. https://doi.org/10.1016/0012-821X(83)90164-4.
Tullborg, E.-L., Smellie, J.A.T., MacKenzie, A.B., 2004. The use of natural uranium decay series studies in support of understanding redox conditions at potential radioactive waste disposal sites. In: Material Research Society, (MRS), vol. 807. Scientific basis for Nuclear Waste Management XXVII, pp. 571–576. https://doi.org/10.1557/PROC-807-571.
Tullborg, E.-L., Drake, H., Sandström, B., 2008. Palaeohydrogeology: a methodology based on fracture mineral studies. Appl. Geochem. 23, 1881–1897. https://doi.org/10.1016/j.apgeochem.2008.02.009.
Tullborg, E.L., Suksi, J., Geipel, G., Krall, L., Auqué, L., Gimeno, M., Puigdomenech, I., 2017. The occurrences of $Ca_2UO_2(CO_3)_3^0$ complex in Fe(II) containing deep groundwater at Forsmark, Eastern Sweden. Proc. Earth Planet. Sci. 17, 440–443. https://doi.org/10.1016/j.proeps.2016.12.111.